



ISAE SUPAERO & UNIVERSITÉ PAUL SABATIER

MASTER'S THESIS

# Finding Pulsating Sources In The XMM-Newton Archival Data

Amaury Perrocheau

IRAP & Osservatorio Astronomico Cagliari  
Toulouse, France & Cagliari, Italy

03/04/2023 - 12/09/2023

Supervised by  
Dr. Natalie Webb  
Dr. Matteo Bachetti

## Abstract

*Context.* More than 15000 observations have been made with the European Space Agency X-ray observatory XMM-Newton, yet the nature of most of the sources detected is still unknown. Some of them emit pulsations (like pulsars or X-ray binaries), revealing rare objects that could significantly contribute to our understanding of stellar evolution.

*Aims.* We present here a timing analysis of some observations from the 13th Data Release (DR13) of the XMM-Newton X-ray detection catalogue (4XMM-DR13) in order to identify and characterize new rare compact objects.

*Methods.* I contributed to developing and then running an extensive data analysis pipeline using techniques like epoch folding, Zn-statistic searches, and acceleration searches to identify periodic signals and pulsations. We also performed spectral analysis to understand the X-ray emission properties and determine the source nature.

*Results.* 2359 sources were analyzed from 111 observations. Among them, 34 presented a significant pulsation ranging from 0.14 s to 7468.5 s. Only 14 of these were already known but none of them has been observed to pulsate in the past. The spectral analysis revealed the nature of these unknown sources to be X-ray binaries, powered either by a black hole or a pulsar, AGNs and stars. The detection of pulsations in AGNs revealed potential intermediate mass black hole candidates.

# Table of Contents

<b>1</b>	<b>Introduction</b>	<b>1</b>
1.1	Background information on X-ray astronomy . . . . .	1
1.2	The XMM-Newton observatory . . . . .	2
1.2.1	Instrumentation and capabilities . . . . .	2
1.2.2	Data collection and archival process . . . . .	3
1.3	Importance of uncovering new rare objects . . . . .	4
1.3.1	Compact objects origin . . . . .	4
1.3.2	Classification of potential sources (AGN, stars, X-ray binaries, CVs, ULXs, magnetars, pulsars, gamma-ray bursts, supernovae, etc.) . . . . .	5
1.4	Objectives and scope of the project . . . . .	9
<b>2</b>	<b>Methodology</b>	<b>11</b>
2.1	Overview of existing code and algorithms for pulsation search . . . . .	11
2.1.1	Stingray & HENDRICS . . . . .	11
2.1.2	Fourier Transform . . . . .	11
2.1.3	Epoch Folding . . . . .	12
2.1.4	Acceleration searches . . . . .	13
2.1.5	$Z_n^2$ searches . . . . .	14
2.2	Implementation and pulsating candidates selection . . . . .	15
2.2.1	Processing pipeline . . . . .	15
2.2.2	Analysis pipeline . . . . .	16
2.2.3	Further Analysis . . . . .	16
2.3	Spectral Fitting . . . . .	17
2.4	Test Case : AR Scorpii, a white dwarf pulsar . . . . .	18
<b>3</b>	<b>Results and Discussion</b>	<b>19</b>
3.1	Pulsating candidates . . . . .	19
3.2	Pulse profile of the candidates . . . . .	20
3.3	Spectral fitting . . . . .	22
3.4	Discussion . . . . .	23
3.4.1	On the pulsation's origin in quasars . . . . .	23
3.4.2	Distinction based on $f_X/f_{opt}$ . . . . .	24
3.4.3	Distinction based on the photon index $\Gamma$ . . . . .	25
3.4.4	Black body emission . . . . .	25

3.4.5	Sources with failed spectra fit . . . . .	26
3.4.6	Pulse Profile . . . . .	26
3.4.7	Long period pulsations . . . . .	26
3.4.8	Pulsar emission model . . . . .	27
3.4.9	Pulsar Population . . . . .	28
<b>4</b>	<b>Conclusion and Perspectives</b>	<b>29</b>
<b>A</b>	<b>Code</b>	<b>37</b>
<b>B</b>	<b>Pulse profiles</b>	<b>38</b>
<b>C</b>	<b>Pulsar emission geometry</b>	<b>41</b>

# Chapter 1

## Introduction

### 1.1 Background information on X-ray astronomy

X-ray astronomy is the study of celestial objects that emit in the X-ray part of the electromagnetic spectrum. X-rays are electromagnetic radiation with high energy allowing us to see through interstellar dust and gas as they are transparent to X-rays. They have a typical wavelength of  $10^{-9}$  to  $10^{-11}$  m, which correspond to an energy of  $10^3$  to  $10^5$  eV (The electron volt or eV is a measure of energy equal to  $1.602 \times 10^{-19}$  J corresponding to the change of energy of an electron accelerated in a potential of 1V). X-rays are emitted by high energy processes and they mostly come from the hottest regions of the Universe (from  $10^6$  to  $10^8$  K). The first evidence of X-ray emission was of the corona of the Sun observed in 1948. However, the first source from outside our Solar System was discovered by teams led by Riccardo Giacconi and Bruno Rossi in 1962 : Scorpius X-1, the most powerful X-ray source in the sky after the Sun ([Giacconi et al. \(1962\)](#), [Bowyer et al. \(1964\)](#)). It was later classified as a Low-Mass X-ray Binary (LMXB) ([Steeghs & Casares, 2002](#)), which is a system composed of a compact object (typically a black hole or a neutron star) and a low mass star (see section 1.3 for a detailed explanation).

Because the Earth's atmosphere absorbs X-rays, observations must be made with space based telescopes such as XMM-Newton ([Jansen et al., 2001](#)) or NuSTAR ([Harrison et al., 2013](#)). From an observational point of view, X-ray astronomy must use different optical systems than visible telescopes. Because X-rays are so energetic, they can pass through mirrors, so they must be manufactured of a substance that will reflect an X-ray photon and must be positioned so that the X-rays strike the mirror at a “grazing incidence” to be reflected. The largest angle for which reflection can happen is called the critical grazing angle and is given by  $\theta_c = (4\pi r_0 \lambda^2 n)^{0.5}$ , where  $r_0$  is the classical electron radius,  $n$  the electron density and  $\lambda$  the wavelength of the X-ray radiation (e.g. [Ramsey et al., 1993](#)). For X-ray observations, this angle is typically of the order of hundreds of milli degrees (e.g. [Basu, 2014](#)). Different configurations of optics are possible to observe X-rays, but the most commonly used is the Wolter I configuration ([Wolter, 1952](#)). In order to focus photons onto the detector, it uses two mirrors arranged coaxially and placed on a paraboloid and a hyperboloid. This configuration has several advantages including a shorter focal length than the two other Wolter's configurations and also the possibility to put together many confocal shells in order to increase the effective area (e.g. [Pareschi et al., 2021](#)). As for the detector, CCDs are the most widely used today in X-ray astronomy (onboard XMM-Newton, NuSTAR, Chandra ([Weisskopf](#)

et al., 2000), Swift (Burrows et al., 2005), ...)

## 1.2 The XMM-Newton observatory

### 1.2.1 Instrumentation and capabilities

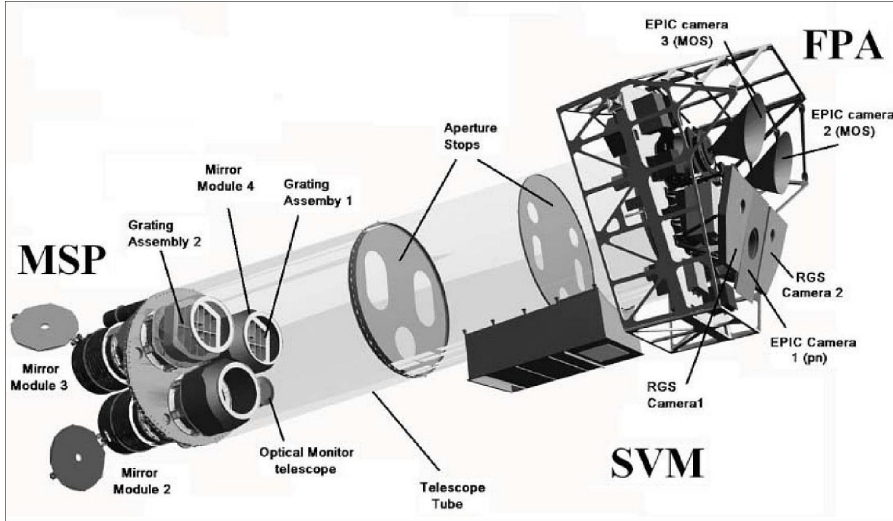


Figure 1.1: Diagram of the XMM-Newton spacecraft, credit :ESA/XMM-Newton

The European Space Agency's (ESA) X-ray Multi-Mirror Mission (XMM-Newton) was launched by an Ariane 504 on December 10th 1999. It is designed to observe soft X-rays from 0.15 to 12 keV (Jansen et al., 2001) that could be coming from star formation, galaxy clusters or accretion onto black holes for instance. XMM-Newton was placed on an elliptical orbit with the following orbital parameters : eccentricity  $e \approx 0.88$ , perigee  $r_p = 7000$  km, apogee  $r_a = 114000$  km, period  $P \approx 48$  hours and inclination  $i = 40^\circ$ . However due to the presence of the Earth's radiation belt, the satellite can only operate when its altitude is above 60 000 km and thus can only observe for about 40 hours out of its 48 hours orbit (Jansen et al., 2001).

XMM-Newton is composed of two individual parts: the three Wolter type-1 X-ray telescopes and a 30-cm optical/UV telescope so that the observer can have simultaneous access to X-ray and optical/UV. There are three X-ray cameras onboard XMM-Newton, constituting the European Photon Imaging Camera (EPIC) (Turner et al., 1998). The first two cameras are MOS (Metal Oxide Semi-conductor) CCD arrays and positioned in the focal plane of the X-ray telescopes (Turner et al., 2001). They receive about half of the incident flux, the other half going to the Reflection Grating Spectrometers (RGS) (den Herder et al., 2001). The third camera is the EPIC-PN instrument and uses pn CCD arrays (?).

The EPIC cameras, MOS and PN, are designed to work in the soft X-ray band, from 0.15 to 12 keV (Ebrero, 2023). They have a field of view (FOV) of  $\approx 30'$  and a spectral resolution of  $E/\Delta E \approx 20 - 50$ .

Different science modes can be used with the EPIC cameras. In this work, as we are focusing on the PN camera because of its better time resolution, we will describe only the modes we used : Full Frame and Small Window. In the Full Frame mode, all pixels from all CCDs are used and it is possible to cover the full field of view and the time resolution is 73.4 ms. The Small Window mode uses only a part of one of the 12 CCDs available with EPIC PN. It is designed to provide higher time resolution (5.7 ms) than the Full Frame mode while maintaining a larger field of view compared to Timing mode ([Ebrero, 2023](#)).

The point-spread function (PSF) is an important parameter to determine the quality of a telescope and it represents how much the observed light distribution has been distorted by the instrument. The exact value of the PSF of the three cameras for various energy is given in [Ebrero \(2023\)](#), but to summarise, the core of its PSF is narrow and varies little over a wide energy range (0.1–6 keV) although it becomes more energy dependent above 6 keV. A second important parameter is the effective area of the telescope which is the mirrors' ability to collect radiation at different photon energies. Although, this parameter varies with the energy, the total mirror geometric effective area at 1.5 keV energy is about  $1550 \text{ cm}^2$  for each telescope (PN and 2 MOS), i.e.,  $4650 \text{ cm}^2$  in total ([Ebrero, 2023](#)).

The sensitivity of XMM depends on the duration of the observation and the background. [Watson et al. \(2001\)](#) gives the sensitivity as a function of exposure time for an assumed  $\alpha = 1.7$  power-law spectrum with a hydrogen column density  $N_H = 3 \times 10^{20} \text{ cm}^{-2}$ . It varies between  $10^{-16}$  and  $10^{-13} \text{ erg cm}^{-2} \text{ s}^{-1}$  for an exposure between  $10^6$  and  $10^3$  s for the three EPIC cameras in the total band (0.2–12.0 keV) soft and hard X-ray bands.

X-ray spectroscopy is performed with the RGS at a high resolution of  $R = \lambda/\Delta\lambda$  between 100 to 500 at Full Width Half Maximum (FWHM) ([den Herder et al., 2001](#)). It uses a set of gratings to disperse the X-ray light and provides detailed spectral information in the energy range 0.33–2.5 keV ([den Herder et al., 2001](#)), allowing for the measurement of energy shifts (displacement of emission or absorption lines from their expected or rest-frame energies [Okun et al. \(2000\)](#)) and line broadening (broadening of the lines by the Doppler effect due to the rapid rotation of an object) caused by motion or extreme gravitational fields. The RGS enables the study of emission and absorption lines from various astrophysical sources, providing insights into the physical processes occurring in hot plasma and accretion disks around compact objects.

The UV/optical telescope onboard of XMM-Newton is the Optical Monitor (OM) ([Mason et al., 2001](#)). It is sensitive to the 180 – 600 nm band and has a field of view of 17 centered on the X-ray field of view. The XMM-OM is based on a Ritchey Chrétien telescope design (e.g. [Wilson, 1996](#)) with a 0.3 m primary mirror feeding a hyperboloid secondary. XMM-OM thus provide simultaneous observations in the optical/UV regime to the XMM-EPIC X-ray observation.

### 1.2.2 Data collection and archival process

All the observations are housed in the XMM Science Archive (XSA) ([Arviset et al., 2002](#)). A robust set of software programs was created especially for the study of XMM-Newton data and is called the XMM-Newton Science Analysis System (SAS) ([Gabriel et al., 2004](#)). For data reduction, calibration, image analysis, spectral fitting, and timing analysis, SAS provides a set of tools and methods.

Two kinds of files are available in the XMM-Newton Science Archive (XSA) :

- Observation Data Files (ODF) : These are the uncalibrated science files and they cannot be directly used for scientific data analysis. One must use reduction tasks from the Science

Analysis Software.

- Processing Pipeline System (PPS) products : These are the result of the SAS reduction pipelines run on the ODF files. These files can be X-ray cameras event lists, source lists, multi-band images, background-subtracted spectra and light curves. These are the files used for scientific analysis.

In this work both ODF and PPS files were used, in particular event lists, spectra and light curves. Event lists are datasets containing information about the photons recorded by the X-ray detectors (PN, MOS1, or MOS2), which includes the photon time of arrival, the energy and the position on the detector for the whole field of view. Spectra are source specific and are the distribution of the source photons as the function of energy. Lightcurves are also source specific and provide the number of photons as function of time.

## 1.3 Importance of uncovering new rare objects

XMM-Newton is the X-ray observatory with the largest collecting area that has ever been launched. Among the 15000 observations to date, many of the X-ray detections are compact objects and we describe here the different types of compact objects that can be present in the catalog.

### 1.3.1 Compact objects origin

The life cycle of a star starts with the gravitational collapse inside a gas cloud forming a protostar (e.g. [Kunitomo et al., 2017](#)). It then enters the main sequence phase, when the star undergoes fusion of hydrogen in its core. Lifespans for main sequence stars have a vast range : a  $1 M_{\odot}$  star will spend 10 billion years on the main sequence while a  $10 M_{\odot}$  star will only last 20 million years on the main sequence (e.g. [Zakhzhay, 2013](#)). When too little hydrogen remains in the core of the star for fusion to continue, the star will evolve, depending on its mass, and will then form various objects ([Iben, 1974](#)). For stars with masses  $M < 10 M_{\odot}$ , they will form a planetary nebula and a white dwarf : a low luminosity (from  $10^{-5} L_{\odot}$  to  $1 L_{\odot}$  depending on its age) and compact object with a mass on the order of that of the Sun, but with a radius comparable to that of the Earth (e.g. [Koester, 2013](#)).

For stars with a mass greater than  $10 M_{\odot}$ , they will end their main sequence lives in a powerful explosion called a supernova (e.g. [Belczynski & Taam, 2008](#)). The shock wave produced by the explosion interacts with the surrounding medium and emits in the X-ray. XMM-Newton's high sensitivity and spatial resolution enable the detection and characterization of these supernovae and help provide information about the energy release and the composition of the supernova ejecta. XMM-Newton can also be used to study supernova remnants (SNRs), the structures formed after the supernova explosion ([Cassam-Chenaï et al., 2004](#)).

For single stars with masses  $10 M_{\odot} < M < 25 M_{\odot}$ , the remnant of the supernova is a neutron star. These are compact objects of about  $1.5 M_{\odot}$  but with a radius of around 12 km (e.g. [Lattimer & Prakash, 2004](#)) . Neutron stars are very dense (approximately  $10^{17} \text{ kg/m}^3$  [Collazos \(2023\)](#)) and are often observed as radio pulsars possess brief (e.g. [Vidana, 2018](#)).

Finally for single stars with masses  $M > 25 M_{\odot}$ , the object left after the supernova can be a black hole : the object collapses to such a small size that not even light can escape from it (e.g. [Fryer, 1999](#)). Matter from the interstellar medium or neighboring stars can fall towards the black

hole, creating an accretion disk. Accretion occurs as matter loses angular momentum due to friction in the disc and falls towards the central compact object. In the innermost regions, the material can reach temperatures of more than a million degrees thus emitting X-rays (e.g. Frank et al., 2002). Compact objects are strong sources of X-ray emission due to various phenomena described below.

### 1.3.2 Classification of potential sources (AGN, stars, X-ray binaries, CVs, ULXs, magnetars, pulsars, gamma-ray bursts, supernovae, etc.)

The categorization of potential sources detected through the utilization of the XMM-Newton observatory is an essential process towards comprehending the inherent characteristics and traits of these objects. The sources can be classified in numerous categories, namely active galactic nuclei (AGN), stars, X-ray binaries, cataclysmic variables (CVs), ultra-luminous X-ray sources (ULXs), magnetars, pulsars, gamma-ray bursts (GRBs), supernovae, and other exotic objects (Tranin et al. (2022), Wilkes et al. (2022)) .

#### Stars

The production of X-ray radiation by stars can be attributed to various astrophysical phenomena, including the presence of stellar coronae (Testa et al., 2015), magnetic activity (Schröder et al., 2008), or binary interactions. The X-ray spectra and variability patterns provide insights into stellar properties, such as magnetic activity, stellar winds, and accretion processes (Testa, 2010).

#### AGNs, Extreme Mass Ratio Inspirals (EMRIs) and merging galaxies

The most probable objects to be observed are active galactic nuclei (AGN) (e.g. Gallo et al., 2023), a small area at the center of some galaxies that is far brighter than the stellar population alone can account for (e.g. Padovani et al., 2017). The rest of the galaxy cannot compete with the core region's radiation output, which is exceedingly bright : between  $10^7 L_\odot$  for some nearby galaxies to  $10^{14} L_\odot$  for the most powerful quasars (Fabian, 1999). From radio waves to gamma rays, AGNs release radiation that spans the whole electromagnetic spectrum. The center supermassive black hole (with a mass greater than  $10^6 M_\odot$ ), consumes material through its accretion disk. As the matter falls towards the supermassive black hole, it emits large quantities of X-rays. AGN are known for exhibiting distinctive X-ray spectra (broadband spectrum, power-law component, Fe K $\alpha$  line) and frequently demonstrating variability across a range of temporal scales (Padovani et al., 2017). ‘Active galaxy’ refers to a galaxy that is home to an AGN (Tadhunter, 2008). The AGN has a great impact on its host galaxy and they have a co-dependent evolution (e.g. Murray et al., 2009)

Extreme mass ratio inspirals (EMRIs) refer to the orbit of a light compact object such as a black hole or a neutron star around a much heavier one, that gradually spirals in due to the emission of gravitational waves. The ratio of their mass is usually greater than 10 000, and this kind of system can be found at the center of galaxies where supermassive black holes reside (Amaro-Seoane et al. (2007), Amaro-Seoane (2018)). Investigating these systems allows scientists to understand the process behind the formation of supermassive black holes.

Galaxies can merge when they collide due to gravitational interactions. Because of these interactions and the friction between the gas and dust, number of processes are triggered. Depending on the galaxies sizes or speeds, star formation rate increases and the previous stellar structures can

be lost, releasing a large amount of energy (Ellison et al., 2022). Observing these mergers allow us to studies the formation and evolution of galaxies over time.

Both EMRIs and merging galaxies can emit pulsations in the X-ray domain. First is when the compact object falling into the SMBH during an EMRI is a pulsar, we are to observe its pulsation. This will provide information about the properties of the pulsar itself but also about the SMBH (Kimpson et al., 2019). During a galaxy merger, transients like X-ray and gamma-ray bursts can happen and exhibit periodic variations because of the accretion processes (Foord et al., 2022).

Studying these two events will be beneficial on several topics. In the case of EMRI, as the compact object crosses the disk, it creates a burst of light. Over the course of an hour, the bursts can repeat periodically. It will emit gravitational waves allowing us to probe the nature of gravity in the strong-field regime predicted by general relativity (McWilliams et al., 2014). The merger of two galaxies will lead to the growth of the central SMBH and trigger AGN phenomena like quasi-periodic eruptions for instance (Metzger et al., 2022). During these events, we will observe a change in the star formation rate, the dark matter distribution and the gas dynamics (Tam et al., 2020), allowing the astronomers to gain insight on the history of the galaxies.

### Pulsars and magnetars: Properties and characteristics

Another probable source of X-ray pulsations are pulsars and magnetars, even though only 5-7 % of the  $\approx 3400$  known pulsars have been observed in X-rays (Vahdat et al., 2022). Pulsars are rapidly rotating neutron stars that were first detected in 1968 (Hewish et al., 1968) and that emit beams of radiation, which can be detected as periodic X-ray pulses. These are a type of neutron star characterized by strong magnetic fields (from  $10^8$  G for millisecond radio pulsars to  $10^{15}$  G for magnetars (e.g. Igoshev et al., 2021), (e.g. Kaspi & Beloborodov, 2017)) and rapid rotation (the rotation period ranging from 1 ms to 10 ms for millisecond pulsars and from 0.3s to 15 s for ‘normal’ pulsars Manchester (2017)). These pulsations can only be observed when the pulsar’s rotation axis and magnetic axis are not aligned (Sasaki et al., 2012) and when the beam crosses the observers line of sight. Depending on the emission mechanism (rotation powered Beskin et al. (2015), accretion powered Nagase (1989) or even both Papitto et al. (2013)), the periodic burst can be observed across different wavelengths, from radio to X-rays and their pulse profiles can be of different shapes (peaks, sinusoids, multiple peaks, symmetry ...) (Sasaki et al. (2012), Jain & Paul (2011)).

Because pulsars have a mass of about  $1.35M_{\odot}$  and a rapid spin rate, they have an extremely large angular momentum. Thus, large external torques are required to alter the spin rate appreciably, making them extremely stable oscillators (Phinney, 1992), and they can be used as clock for the study of astronomical events like gravitational waves or spacecraft navigation (Wang et al., 2023). However they are observed to spin down with time (around  $10^{-15} \text{ s.s}^{-1}$ ) as their energy is converted into magnetic dipole radiation, relativistic particles, high-energy radiation and gravitational waves (Yue-zhu et al., 2016).

Detecting their pulsations can be tricky because of glitches and timing noises. Although pulsars exhibit a regular slowdown (between  $10^{-21}$  and  $10^{-9} \text{ s.s}^{-1}$  Salvo & Sanna (2021)) on their period because of the emission of electromagnetic radiation, some unpredictable changes in their period can be observed : glitches and timing noises. The first phenomenon is a sudden acceleration of the rotation rate ( $\Delta\nu/\nu$  between  $10^{-9}$  and  $10^{-5}$  Lyne et al. (2000)) with a relaxation phase following. It is believed to come from the interaction of the fluid inside the neutron star with its crust (Zhou et al., 2022). The second phenomenon is the stochastic wandering of pulse arrival times that takes the form of red noise (noise which has higher intensity at lower frequencies). These two effects can

make it more complicated to detect pulsations in the light curve (Lyne et al., 1995).

XMM-Newton has played a significant role in the discovery and study of pulsars and magnetars (Mereghetti et al., 2008), providing precise timing measurements, helping to unravel their physical properties and detecting rare objects such as Anomalous X-ray Pulsars (AXP) (Göhler et al., 2005) and Soft Gamma-ray Repeaters (SGRs) (Mereghetti et al., 2005).

Studying these pulsating sources can help us understand their evolution in the  $P - \dot{P}$  diagram (figure 1.2) (Johnston & Karastergiou, 2017) but also investigate the behavior of matter inside extreme environment such as the intense magnetic field of a magnetar (Suh & Mathews, 2010). Moreover, very regular pulsing signals can act as real-world test beds for theories of gravity (Kramer et al., 2021). By monitoring millisecond pulsars, we can detect low-frequency gravitational waves (between  $10^{-10}$  and  $10^{-6}$  Hz) through Pulsar Timing Array (PTA) which measure the small variations in the times of arrival (ToA) of the pulses induced by gravitational waves (Maiorano et al. (2021), Hobbs & Dai (2017)).

### X-ray Binaries and Cataclysmic Variables (CVs)

X-ray binaries are a subclass of binary stars (system in which two stars orbit around a common center of mass) that are bright in X-rays. The accretor, a neutron star or black hole, accretes matter from the companion star, often through an accretion disk (e.g. Reig, 2011). The donor star's evolutionary stage, the mass disparity between the stellar components, and their orbital spacing all affect the lifespan and mass-transfer rate in an X-ray binary (Tauris et al. (2000), Verbunt & Rappaport (1988)). We can distinguish several types of X-ray binaries, classified by the mass of the donor. First, there are the low-mass X-ray binaries (LMXBs). In these systems, the donor star might be a main sequence star, an evolved star (red giant) or a degenerate dwarf (white dwarf) (e.g. Steeghs & Casares, 2002). Then there are the high-mass X-ray binaries (HMXBs). This term refers to a pair of stars with significant X-ray emission in which one of the stars is often a massive star, such as an O or B star, a blue or red supergiant (e.g. Tan, 2021). This massive star dominates the emission in the visible range, while the compact object dominates the X-ray emission. Matter from stellar wind of the massive star can be accreted by the compact object, resulting in X-ray emission. Thanks to XMM-Newton, the characterization of their X-ray spectra, variability patterns, and the nature of the accretion process has improved significantly (e.g. Fragkos, 2011).

HMXBs can serve as a reliable indicator of recent star-formation activity in their host galaxy (Mineo et al., 2011). We can use these sources to define the initial mass function (IMF). By observing only the brightest stars in a galaxy, astronomers are making assumptions about the hidden stellar population by assuming the shape of the IMF to be similar to the measured IMF in the Milky Way. However, recent studies suggest systematic variations of the IMF in elliptical galaxies. This is done by examining the number of LMXBs compared to the number of low-mass stars, enabling a comparison of the IMF shape in different galaxies (Peacock et al., 2014).

Another source of X-rays is cataclysmic variables (CVs). These are a subclass of X-ray binary composed of a white dwarf primary and a mass-transferring secondary. Because the stars are so close to one another (their orbital period can go as low as around 80 min Southworth et al. (2010)), the white dwarf's gravitational pull bends the companion star (Smith, 2007). As a result, the donor star fills its Roche-Lobe (region around a star in a binary system within which orbiting material is gravitationally bound to that star) transferring its hydrogen-rich material through an accretion disk or an accretion flow (e.g. Lin et al., 1985). The loss of gravitational potential energy from the infalling material drives the X-ray emission that is frequently observed from the accretion disc.

Periodic variability due to the orbital motion of the binary system can be observed ([Smith, 2007](#)). The white dwarf itself has been observed to emit pulsations in two systems ([Pelisoli et al. \(2023\)](#), [Schwope et al. \(2023\)](#)) and has been qualified as a white dwarf pulsar as a result.

In such binary systems, the dynamic is determined through various parameters, including the orbital period, the eccentricity, the masses of the components, the inclination angle or the accretion rate. Determining these parameters can help us understand their behavior and mechanisms like the mass transfer (it can be via stellar winds or Roche lobe overflow for instance) or tidal interaction ([McCray & Hatchett \(1975\)](#), [Iben \(1974\)](#), [Podsiadlowski et al. \(2002\)](#)). Accurate timing measurements allow for the determination of the orbital period with high precision, providing insights into the separation, mass ratio, and stability of the binary system ([Pearlman et al., 2019](#)). The eccentricity is giving information about the nature of interactions between the two objects and can influence accretion processes and variability ([Townsend et al., 2011](#)).

### **ULXs and their nature**

There are about 1800 ultraluminous X-ray source (ULX) known (e.g. [Walton et al., 2021](#)). These objects are characterized by the emission of X-rays exceeding the Eddington limit ( $L_{Edd} \approx 3.2 \times 10^4 (\frac{M}{M_\odot}) L_\odot$ ) for a stellar-mass black hole ([Misra et al., 2020](#)). The number of ULXs in a Galaxy is observed to be correlated to the star formation rate (SFR) (e.g. [Bernadich et al., 2022](#)). The mechanisms that allow ULXs to emit such powerful radiation remain unclear. It is now suggested that they could be powered by super-Eddington accretion but the physical mechanism describing super-Eddington accretion is as yet unknown ([Brice et al., 2021](#)).

Recently, some of these systems have been observed pulsating, revealing that some are actually powered by neutron stars and correspond to times of high accretion in the lifetime of a X-ray binaries ([Quintin et al. \(2021\)](#), [Mushtukov et al. \(2020\)](#), [Bachetti et al. \(2014\)](#)). These pulsating ULXs (PULXs) have extreme luminosity (about  $10^{41}$  erg/s), exhibit sinusoidal pulse profiles and are observed to spin up fast. However, their magnetic fields are still unknown.

Even though these objects are extremely luminous, they are also very far away (extragalactic objects) [Bernadich et al. \(2022\)](#). Most of the known ULXs observed with XMM-Newton present a count rate too low to detect any pulsation in their light curve. Adding to the fact that their period derivative is important, some of the known PULXs are observed to be transients ([Hameury & Lasota, 2020](#)). As a result, the number of PULXs detected to this day is still low (< 10, [MacKenzie et al. \(2023\)](#), [Mushtukov et al. \(2020\)](#)), thus the need to find new systems to improve our understanding of them.

Gamma-ray bursts (GRBs) are brief (10 ms to a few hours [Kouveliotou et al. \(1993\)](#)) and extremely energetic events that either come from the death of a high-mass star or from the merger of binary neutron stars (e.g. [Piran et al., 2013](#)). Although XMM-Newton is not suited to observe gamma rays (which have an energy greater than roughly 100 keV), it has been very useful to observe the “afterglow” of these events providing insights into the emission mechanisms, energy release, and environment surrounding the GRB source ([Grupe et al., 2007](#)).

All of these objects are very important for astrophysics, as they can give us information about the formation and evolution of compact objects, stellar populations, accretion physics and gravitational waves. One of the ways to identify and study these rare objects is to search for pulsations in their X-ray emission. Pulsations are periodic variations in the intensity of the radiation that can be caused by various mechanisms, such as rotation, orbital motion or magnetic field. Pulsations can reveal important information about the source properties, such as mass, radius, magnetic field

strength, spin period, orbital period and companion star. However, finding pulsating sources in X-ray is not easy, as they are often faint and obscured by noise or other sources but this will enable us to discover new rare sources.

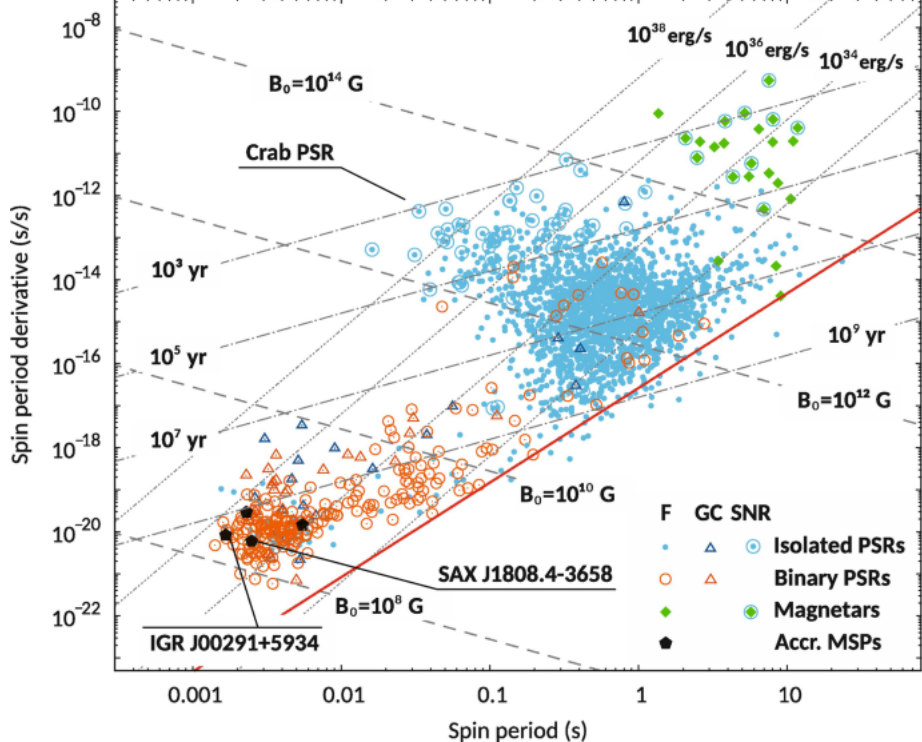


Figure 1.2:  $P - \dot{P}$  diagram of rotation-powered pulsars (blue and orange symbols refer to isolated and binary pulsars , respectively), accreting MSPs (black pentagons) and magnetars (green diamonds). Diagram from [Salvo & Sanna \(2021\)](#)

## 1.4 Objectives and scope of the project

The main goal of this project is to uncover new rare objects by searching for pulsations in the whole of the XMM-Newton archival data. This project aims to use the HENDRICS and Stingray ([Bachetti et al. \(2022\)](#) [Huppenkothen et al. \(2019\)](#) [Huppenkothen et al. \(2019\)](#)) packages to perform a systematic and comprehensive search for pulsations on more than 20 years of XMM-Newton observations. This code searches for pulsation using acceleration searches, epoch folding and  $Z_n^2$  statistics techniques (see chapter 2 for a thorough description).

Throughout this work we used pulsar timing to detect unknown sources in the archival data of XMM-Newton. This powerful technique accounts for every rotation of pulsar over the observation data set and allow us to search for gravitational waves, infer the masses of neutron stars, test general relativity. Because pulsations have different shapes depending on their spin properties and on the viewing angle of its beam, there is no one-fits-all technique to measure their pulsation.

The project also aims to analyze the pulsating candidates, verify the pulsations and determine the source nature, through fitting X-ray spectra and multi-wavelength data analysis. This project is motivated by the scientific importance of finding new pulsating sources in X-ray, as they can help us understand more about these populations and their physical processes. Identifying new compact objects is also important for understanding the initial mass function of stars, as knowing the compact object nature allows us to understand the type of stars that were present in the early Universe. Further, determining the nature of the compact object in ULXs, X-ray binaries or CVs helps us understand stellar evolution and also understand the nature of the accretion that takes place in these systems. With accurate timing data, it is also possible to constrain the binary parameters. Finally, identifying extreme mass ratio inspirals (EMRIs) or merging galaxies is important as input for future gravitational wave observatories such as LISA ([Amaro-Seoane et al., 2017](#)), ([Moore et al., 2017](#)).

# Chapter 2

## Methodology

### 2.1 Overview of existing code and algorithms for pulsation search

#### 2.1.1 Stingray & HENDRICS

This work used the Python package Stingray ([Bachetti et al., 2022](#); [Huppenkothen et al., 2019](#); [Huppenkothen et al., 2019](#)). This software has been developed for analyzing astronomical light curves and performing time series analysis. It offers a wide range of functionalities, including various Fourier analysis techniques, pulsar data analysis, data simulation, and statistical modeling. The current capabilities of Stingray encompass loading event lists from popular missions like NuSTAR/FPM or XMM-Newton/EPIC. With this software it is possible to construct light curves from event data and perform various operations on light curves. The library supports multiple operations including but not limited to : Good Time Interval (GTI) operations, power spectra with different normalizations, averaged power spectra, maximum likelihood fitting of periodograms and parametric models or quasi-periodic oscillation searches. The most relevant feature for this work is the possibility to do pulsar searches with Epoch Folding and the  $Z_n^2$  test.

The HENDRICS package ([Bachetti, 2018](#)) incorporates command line scripts using the functionalities of the Stingray package.

These packages have been used to find pulsating ULXs (e.g. [Quintin et al., 2021](#)), Quasi Periodic Oscillations (QPOs) (e.g. [Chen et al., 2023](#)) or investigate accretion mechanism in ULX (e.g. [Ghosh & Rana, 2023](#)).

#### 2.1.2 Fourier Transform

Timing analysis studies the temporal patterns and variations of X-ray emissions and can be done through several techniques. The Fourier transform, which enables the breakdown of a time series into its frequency components, is one extensively used method. Astronomers may determine the fundamental frequency, harmonics, and other spectral properties connected to the object periodic behavior pulsar's spinning period by applying the Fourier transform to the light curve. For a set of  $N$  observations  $\{x_i\}_{i=1}^N$  taken at times  $\{t_i\}_{i=1}^N$  (the time resolution being  $\Delta t = T/N$  with  $T$  the

total duration of the observation), the amplitude  $a_k$  of the Fourier transform at the frequency  $\nu_k$  is given by the following equation :

$$a_k = \sum_i x_i \exp(2i\pi\nu_k t_i) \quad (2.1)$$

The set of frequencies  $\{\nu_k\}_k$  must be carefully chosen depending on the total duration of the observation  $T$  and the spacing between two data points  $\Delta t$ . In fact we can not infer a period longer than the total duration of the observation, thus the smallest frequency is  $1/T$ . In practice, we choose a multiple (i.e 4 or 5) of this frequency as the lower bound of the frequency, so that we can detect a few repetitions of the pulsation in the observation. We can't resolve periods shorter than  $\Delta t/2$ , giving us the maximum frequency : the Nyquist frequency  $0.5/\Delta t$ .

From the Fourier transform, we can compute the periodogram, it is an estimate of the power spectral density (PSD), and tells us how much power there is in a certain frequency. It is given by the following equation :

$$P_k = |a_k|^2 \quad (2.2)$$

There are a number of ways to normalize the periodogram depending on its use but they will not be covered here (see for instance the Leahy normalization ([Leahy et al., 1983](#)) or the Welch/Bartlett normalization ([Welch, 1967](#))). However, we used a special kind of periodogram in this work : the Lomb Scargle periodogram ([Lomb \(1976\)](#), [Scargle \(1982\)](#)). Its advantage is to be compatible with unevenly sampled data and is given by the following formula :

$$P_{LS}(\nu) = \frac{1}{2} \left[ \left( \sum_i x_i \cos 2\pi\nu(t_i - \tau) \right)^2 / \sum_i \cos^2 2\pi\nu(t_i - \tau) + \left( \sum_i x_i \sin 2\pi\nu(t_i - \tau) \right)^2 / \sum_i \sin^2 2\pi\nu(t_i - \tau) \right] \quad (2.3)$$

with

$$\tau = \frac{1}{4\pi\nu} \tan^{-1} \left( \frac{\sum_i \sin(4\pi\nu t_i)}{\sum_i \cos(4\pi\nu t_i)} \right) \quad (2.4)$$

Unfortunately, Fourier transform has limitations primarily related to the presence of noise in the data. [Lazarus et al. \(2015\)](#) demonstrated that Fourier transform has a vulnerability to red noise and thus limit the possibility to detect long period pulsations ( $P > 1s$ ). As a result, a selection bias appears if we only rely on Fourier transform techniques to detect pulsations.

### 2.1.3 Epoch Folding

Another important technique is epoch folding, which involves folding the pulsar's data over its known or estimated period and summing the signal within each phase bin. We can have an estimate of the period with the Fourier transform and the periodogram. By aligning the data based on the pulsar's period, epoch folding enhances the signal-to-noise ratio (SNR), making it easier to detect weak or sporadic pulsations. This method is beneficial for studying pulsars with irregular or evolving periods.

In practice, we select a range of periods around the estimated one and fold the light curve for every trial period. To find the period that gives the “best” pulse profile we can compute the  $\chi^2$  statistics by comparing with a flat model using equation [2.5](#).

$$S = \sum_i \frac{P_i - \bar{P}}{\sigma^2} \quad (2.5)$$

where  $P_i$  is the pulse profile of the trial period in bin  $i$ ,  $\bar{P}$  is the mean level of the profile, and  $\sigma$  is the standard deviation. If there is no pulsation, the  $S$  will follow a  $\chi_{n-1}^2$  distribution where  $n$  is the number of bins in the folded profile. If there is actually a pulsation, we will observe a deviation in the statistic. We can define a threshold  $\epsilon$ , to consider a peak an actual candidate. But close to the correct frequency the peak in the epoch folding periodogram has the shape of a sinc squared function (Leahy et al., 1983).

Although the SNR is increased by folding the light curve, this search technique remains sensitive to red noise (Cameron et al., 2017).

Both Fourier transform and epoch folding techniques are susceptible to the presence of noise, which can obscure or distort the pulsar signal. Random noise sources, such as instrumental noise or background noise, can introduce fluctuations and false detections in the Fourier power spectrum or folded pulse profile. This noise can significantly affect the accuracy of period determination and the estimation of spectral features, leading to uncertainties in the derived pulsar parameters.

The Fourier transform assumes stationarity in the signal, meaning that the properties of the signal remain constant over time. However, pulsar signals can be subject to non-stationary effects, such as pulse profile variations, frequency evolution, and intermittency. These non-stationary behaviors can complicate the interpretation of the Fourier power spectrum and may require more advanced techniques to accurately characterize the timing properties.

#### 2.1.4 Acceleration searches

Acceleration searches is a technique used to find pulsations in binary systems. In such systems, because of the orbital motion and Doppler effect, the observed pulsation will be spread out over a range of frequencies if the observation duration is longer than the orbital period  $P_{orb}$  (Andersen & Ransom, 2018). For this reason, it is complicated to find pulsations in short period systems with Fourier techniques.

One solution is to assume a constant acceleration of the pulsar over a small fraction of its orbit ( $< P_{orb}/10$ ) so that we will observe its spin frequency to drift linearly over this time. We can then re-sample the time series using equation 2.6 to be placed into an inertial frame of reference where the pulsar is at rest (Johnston & Kulkarni, 1991).

$$T = t \left( 1 + \frac{v(t)}{c} \right), v(t) = at \quad (2.6)$$

After the time series have been re-sampled and the Doppler effect corrected, we can run a Fourier search to find the pulsation. However, one has to assume a value for the acceleration, this kind of technique iterates and searches over a range of acceleration and orbit form. For each acceleration trial, one has to re-sample the time series and compute its Fourier transform, which is computationally heavy.

An alternative is to compute the acceleration searches in the Fourier domain (Ransom et al., 2002). When assuming a constant acceleration, we consider a linear drift of the spin frequency  $f$ , which means that the frequency derivative  $\dot{f}$  is constant Dimoudi et al. (2018). The signal frequency has drifted over  $z$  Fourier bins during the observation time  $T$  so that we can write :

$$a = \frac{\dot{f}}{f_0} c = \frac{zc}{f_0 T^2} \quad (2.7)$$

where  $f_0$  is the frequency in the rest frame.

Instead of stretching the signal, we can correct the Fourier response in the  $f - \dot{f}$  plane using the number of bins that we assumed the frequency has drifted  $z$ . This correction is described in details in [Ransom et al. \(2002\)](#).

### 2.1.5 $Z_n^2$ searches

The  $Z_n^2$  search is a statistical method used in pulsar timing analysis to identify periodic signals and measure their significance. It is particularly effective for detecting pulsations with unknown periods or periods that are changing over time ([Buccheri et al., 1983](#)).

The  $Z_n^2$  statistic is derived from the folding of the data over a trial period, similar to the epoch folding technique however it has high values when the signal is well described by a small number of sinusoidal harmonics :  $n$  ([Bachetti & Huppenkothen, 2022](#)). Let's consider  $\{t_j\}_{j=1}^N$  the times of detection of  $N$  photons. Given a pulse frequency  $f$  and its time derivatives  $\dot{f}, \ddot{f}, \dots$  we can define the phase of photon  $j$  as

$$\Phi_j = \Phi_0 + 2\pi f t_j + \frac{1}{2} 2\pi \dot{f} t_j^2 + \dots \quad (2.8)$$

The  $Z_n^2$  statistic is then given by :

$$Z_n^2 = \frac{2}{N} \sum_{k=1}^n \left[ \left( \sum_{j=1}^N \cos(k\Phi_j) \right)^2 + \left( \sum_{j=1}^N \sin(k\Phi_j) \right)^2 \right] \quad (2.9)$$

The  $Z_n^2$  statistic is expected to have a value close to zero for random noise and background signals, while a significant non-zero value indicates the presence of a coherent periodic signal. By calculating the  $Z_n^2$  statistic for a range of trial periods, we can search for the period that yields the highest  $Z_n^2$  value. Far from the pulsation, the  $Z_n^2$  statistics follows a  $\chi_{2n}^2$  distribution, thus we can set a threshold to asses the significance of a peak over some noise.

When computing the  $Z_n^2$  for a single harmonic  $n = 1$ , it is called the Rayleigh test ([Mardia \(1975\), Gibson et al. \(1982\)](#)). In order to know which number of harmonics best describes the profile, one should perform the H-test ([de Jager & Büsching, 2010](#)). It is defined as :

$$H = \max(Z_m^2 - 4m + 4), m \text{ in } [1, N_{max}] \quad (2.10)$$

where  $N_{max}$  is the maximum number of harmonics one wants to investigate. The value of  $Z_m^2$  is increasing with  $m$  as the number of degree of freedom is increasing, thus the need to correct by a factor  $4(m - 1)$ .

The  $Z_n^2$  search has an edge over Fourier transform and epoch folding as it does not require prior knowledge of the pulsar's period, making it suitable for detecting unknown periods. It is also less affected by the presence of noise and non-stationary effects compared to other methods. However, it should be noted that the  $Z_n^2$  search may still be sensitive to noise and other systematic effects.

## 2.2 Implementation and pulsating candidates selection

All of the techniques mentioned above are implemented in Stingray. This worked is based on a processing pipeline written by Matteo Bachetti prior to the start of the project. Figure 2.1 describes the architecture of the pulsating candidates selection and analysis pipeline.

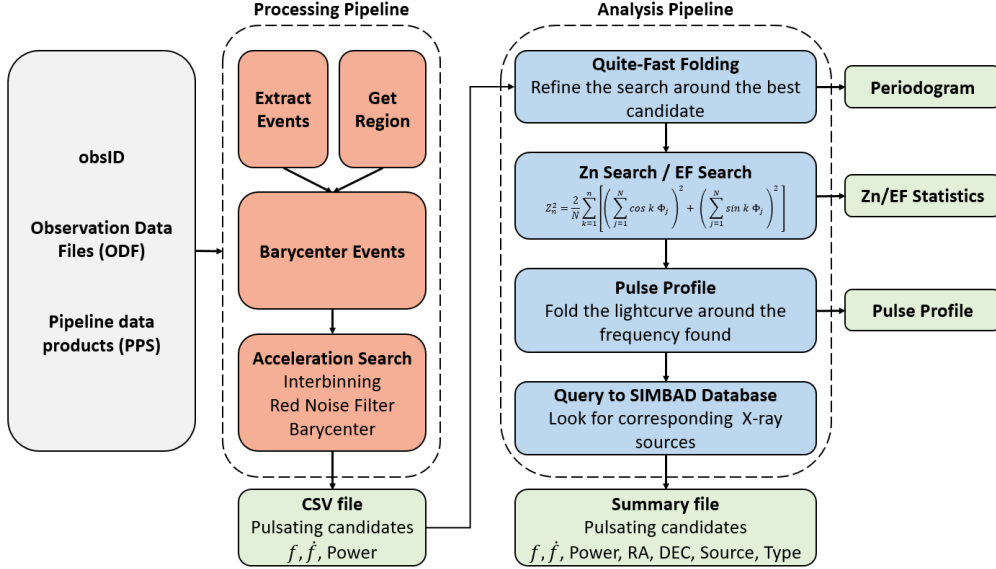


Figure 2.1: Architecture of the pulsating candidates selection and analysis pipeline

### 2.2.1 Processing pipeline

First, the processing pipeline is taking the ODF and PPS of an observation characterized by its obsID. Each source detected in the observation with more than 100 EPIC counts was automatically processed by the SAS pipeline. The processing pipeline uses the same sky region (circle around the position of the source in right ascension (RA) and declination (DEC)) as the SAS pipeline. It extracts the events and barycenters them using tasks from the SAS. The barycenter task shifts the arrival time of a photon as if it would have been detected at the barycenter of the solar system instead of the position of the satellite. Doing so corrects for the effects of the motion of the spacecraft and the Earth's motion around the Solar System barycenter.

The Fourier domain acceleration search was applied to both the raw and barycentered time series. By doing so, we are able to see if a pulsation is only detected because of the motion of the spacecraft or if it is inherent to the signal. We set the searching range between  $\frac{4}{\text{obs duration}}$  and  $\frac{2}{\text{frame rate}}$  to account for the Shanon criterion and to avoid detecting candidates whose pulsation would be the whole duration of the observation. The output of the acceleration is basically a periodogram. In the frequency space, a loss of sensitivity is happening at frequencies close to the borders of the spectral bins. A method called “interbinning” consists of approximating the Fourier response at half-bin frequencies by the interpolation given in equation 2.11 (Lorimer &

Kramer (2004), Middleditch et al. (1993)). Unfortunately, this method produces a lot of spurious candidates.

$$F_{k+1/2} \approx \frac{\pi}{4}(F_k - F_{k+1}) \quad (2.11)$$

To the existing pipeline, I improved the red noise filter. The red noise is an important problem as the lower limit of the frequency range is low (because the observation duration is long). A way to deal with it is to rescale the Fourier transform given by the acceleration search. The Python code for this function is given in appendix A. It should be noted that this method is experimental and can remove a lot of candidates.

Both the interbinning and red noise filter are applied to the raw and barycentered time series, producing 6 different lists of candidates for each sources : raw (*resp.* *barycentered*), raw (*resp.* *barycentered*) with interbinning, raw (*resp.* *barycentered*) with red noise filter. These candidates are stored in a csv file, however up to hundreds of candidates are produced in the searching range, thus the need to refine the search.

### 2.2.2 Analysis pipeline

The major part of my work was to develop the analysis pipeline to confirm the pulsation and provide useful information about the source. From all the candidates in the csv file, I select the one with the highest power. As there are often multiple candidates characterizing the same pulsation around the most powerful, I average their frequencies to obtain the starting point of the different searches.

I first execute a version of the folding algorithm known as “quite fast folding algorithm” The pipeline can produce up to hundreds of candidates in the searching range, thus the need to refine the search. From the output csv file, I select the most powerful candidates and its neighbors and run the “quite-fast” folding algorithm to search for the actual best candidate and obtain a periodogram. The  $Z_n^2$  search algorithm is run around the this candidate to obtained the distribution of the  $Z_n^2$  statistics. Significant peaks in this distribution indicates the presence of pulsations. The same applies for the Epoch Folding (EF) search.

We select only the pulsations above a  $3 - \sigma$  threshold and compute the pulse profile for the one with the greatest statistic.

From the coordinates provided in the fits file of the source, we can query to the astronomical database SIMBAD (Wenger et al., 2000) to know if a source have previously been observed and categorized at this position before. Moreover, a search on Vizier (Ochsenbein, 1996) can reveal if the source has been previously observed by other missions and get multi-wavelength observations of it. Information such as the magnitude in several bands, the redshift or the classification of the source are available.

### 2.2.3 Further Analysis

Once an interesting pulse profile is generated, we need to confirm that the pulsation is indeed coming from the source as another one in the field of view could be contaminating.

SAS provide a tutorial<sup>1</sup> to extract a light curve from a PN event list. First, we select several backgrounds close and further away from the source, and we extract their light curve using the SAS task : *evselect*<sup>2</sup>. The source light curve is also extracted using the same command and need to be

---

<sup>1</sup><https://www.cosmos.esa.int/web/xmm-newton/sas-thread-timing>

<sup>2</sup><https://xmm-tools.cosmos.esa.int/external/sas/current/doc/evselect.pdf>

corrected for various effects affecting the detection efficiency, such as vignetting, bad pixels, PSF variation and quantum efficiency. A background subtraction and a correction are made using the task `epiclccorr`<sup>3</sup>

Using the same period the analysis pipeline returned, we fold the raw source, the background and the corrected light curves. If we observe the pulsation only in the background and the raw light curve, then the pulsation might be coming from another source in the field of view.

## 2.3 Spectral Fitting

The spectrum of a source can give us information on its nature. To do so, we fitted the source spectra with models using Xspec (Arnaud, 1996). The ancillary response matrix and the detector response matrix were created by the XMM-SAS task `arfgen` and `rmfgen`. As AGNs are the most abundant X-ray sources, we first tried using known AGN models. Their average spectra is the result of a combination of a power law, a narrow Fe  $K\alpha$  emission line and some reflection (e.g. Corral et al., 2011) although some spectra may present what we call a “soft excess”, which is an excess of radiation below 1 keV (e.g. Boissay et al., 2016). We will follow the strategy used by Corral et al. (2011) to classify AGNs. The first model used is an absorbed power-law taking into account the absorption by hydrogen in our Galaxy along the line of site (Dickey & Lockman, 1990). The corresponding Xspec model is `phabs*powerlaw` and is given by equation 2.12 :

$$A(E) = \exp [-N_H \sigma(E)] K E^{-\Gamma} \quad (2.12)$$

where  $K$  is a normalization parameter in photons/keV/cm<sup>2</sup>/s at 1 keV ,  $\Gamma$  the dimensionless photon index of power law,  $N_H$  the equivalent hydrogen column (in units of  $10^{22}$  atoms.cm<sup>-2</sup>) and  $\sigma(E)$  the photo-electric cross-section.

An other model we tried to fit is a black body spectra. Stars X-ray spectra can be well modeled by this model. By still accounting for absorption, the corresponding Xspec model is `phabs*bbody` and is given by equation 2.13 :

$$A(E) = \exp [-N_H \sigma(E)] \frac{K \times 8.0525 E^2 dE}{(kT)^4 [\exp(E/kT) - 1]} \quad (2.13)$$

where  $K$  is a normalization parameter,  $kT$  is the temperature in kEV and  $N_H$  and  $\sigma(E)$  still have the same signification. In order to asses the goodness of a fit, we consider a threshold of 30% for the null hypothesis probability, meaning that fits with a null hypothesis probability greater than 30% will be considered acceptable.

From the spectral fitting, we can compute the flux in the model energy band. Here, we compute  $f_{0.2-12\text{ keV}}$ , the flux between 0.2 and 12 keV in erg/cm<sup>2</sup>/s. From there, we can obtain an estimation of the source intrinsic X-ray luminosity  $L$  by using equation 2.14 providing we can have an estimate of the distance  $d$ . Such a distance can be found through the detection of a counterpart at other wavelengths (GAIA for instance Gaia Collaboration et al. (2016), Gaia Collaboration et al. (2023)). If no information about its distance is available, we assume a distance of 1 kpc as this is the shortest distance to get out of the Galactic disk from the Solar system.

$$L = 4\pi d^2 f \quad (2.14)$$

---

<sup>3</sup><https://xmm-tools.cosmos.esa.int/external/sas/current/doc/epiclccorr.pdf>

## 2.4 Test Case : AR Scorpii, a white dwarf pulsar

AR Scorpi is a binary system consisting of a white dwarf and a red dwarf. The two stars orbit each other in 3.56 hours (Marsh et al., 2016). In addition, the system has been observed to emit pulsations with a period of 1.97 minutes (Marsh et al., 2016), becoming the first known white dwarf pulsar. As we want to discover new exotic pulsating sources, this object is a good test case for the whole pipeline.

We ran the pipeline on AR Scorpi data (obsID : 0783940101). It detected the expected pulsation and its harmonics. The  $Z_1^2$  statistic and a sinc fit are provided in figure 2.2. The peak reaches well above the detection level set at 99.87 %. The pulse profile has also been computed in both the soft and hard X-ray bands (0.2-2 keV and 2-12 keV) and in the XMM-Newton band (0.2-12 keV). We notice that the pulsation is coming exclusively from the soft X-ray band which is what has been previously found by Takata et al. (2018).

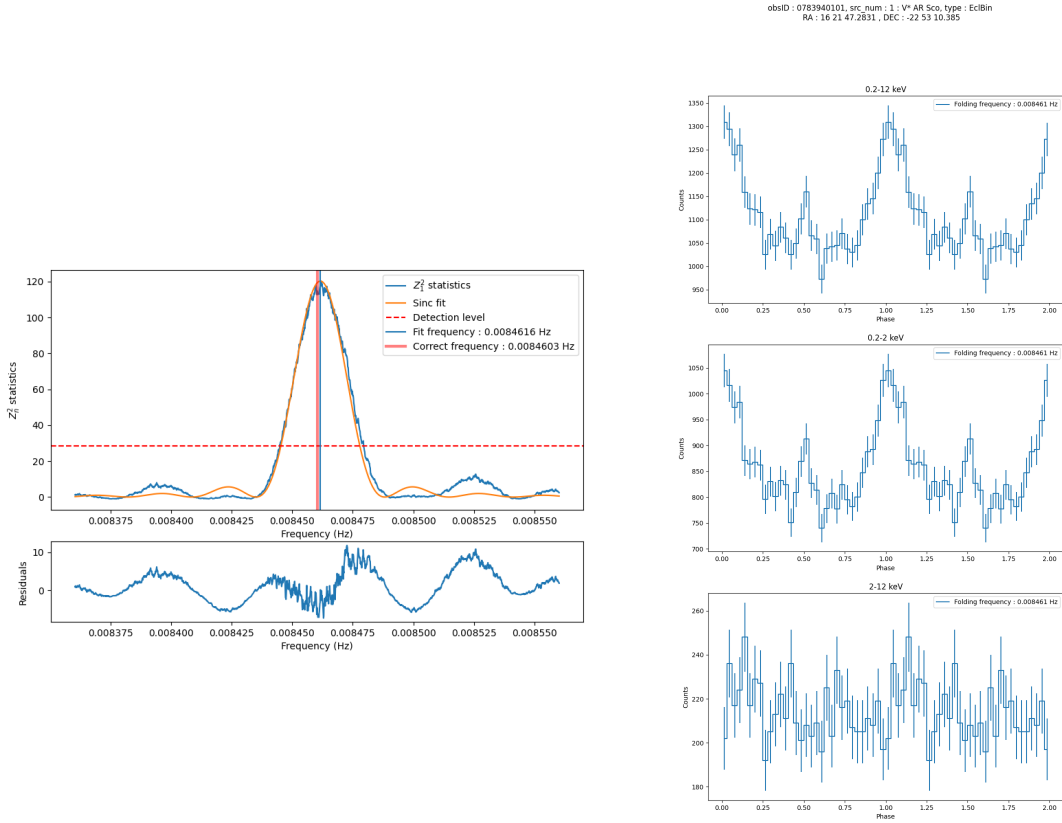


Figure 2.2: Output of the pipeline for the white dwarf pulsar : AR Scorpii. Left :  $Z_1^2$  statistics and a squared sinc fit. Right : pulse profile in different energy bands : 0.2-12keV, 0.2-2 keV, 2-12 keV

# Chapter 3

## Results and Discussion

The pipeline was used on the data coming from XMM-Newton DR13. As of today, 111 observations were processed which correspond to 2359 sources of good enough quality.

### 3.1 Pulsating candidates

Among the 2359 sources, 674 were detected with a pulsation (i.e with a  $Z_n^2$  statistic above the  $3\sigma$  detection level. However, the majority of these are coming from noise or strange flares in there light curve, so we list in table 3.1, only the pulsating candidates detected by the pipeline and that we suspected actually emitting a pulsation after careful examination. We also give their period, coordinates and nature if it is a known source. None of these candidates have been observed to pulsate in the past.

obsID-src	Period s	RA hh mm ss.ss	DEC dd mm ss.ss	Identifier	Nature	P
0860650501-11	0.39	10 24 58.24	-58 57 28.9	Unknown	Unknown	1.42e-5
0860650501-57	0.23	10 26 39.10	-58 52 49.30	Unknown	Unknown	2.33e-4
0860650501-59	0.45	10 26 15.73	-58 52 56.40	Unknown	Unknown	2.92 e-4
0860650501-85	0.62	10 26 41.64	-58 33 32.4	Unknown	Unknown	4.36e-4
0860910601-10	1.18	03 28 31.53	-28 52 51.20	J032831.41-285249.8	QSO	4.69e-5
0862181501-15	0.24	14 32 18.77	+14 44 04.30	Unknown	Unknown	8.13e-7
0862260201-32	2,94	09 28 37.95	+29 57 44.70	Unknown	Unknown	1.00e-8
0862730401-1	0.46	14 47 45.27	+51 48 39.55	J144745.27+514839.5	Seyfert 1	1.26e-5
0862730401-26	0.47	14 45 57.85	+51 37 36.60	Unknown	Unknown	7.50e-7
0862730401-31	0.19	14 47 27.04	+51 42 34.30	Unknown	Unknown	2.31e-7
0862730401-37	0.45	14 47 19.56	+51 44 57.70	Unknown	Unknown	4.83e-6
0862770601-61 <sup>†</sup>	0.14	04 58 22.68	-52 12 27.57	(*)	Star	1.40e-8
0862770701-15	0.41	04 13 38.75	-22 03 54.70	Unknown	Unknown	2.48e-6
0862770701-35	0.41	04 13 32.37	-21 56 52.50	Unknown	Unknown	1.41e-6
0862770801-8	0,30	08 02 14.15	+30 58 34.65	J080214.15+305834.6	QSO	2.03e-4
0862770801-10	0,79	08 02 57.86	+31 07 43.53	J080257.86+310743.5	QSO	4.23e-6
0862900201-1	7416.9	16 16 39.57	+09 31 17.10	J161639.57+093117.1	QSO	1.93e-38
0862900201-5	0.16	16 16 24.17	+09 42 19.35	J161624.17+094219.3	QSO	2.50e-5
0862900201-12	7468.5	16 16 47.91	+09 40 40.70	Unknown	Unknown	1.19e-10
0862980101-1	6079.1	03 33 35.42	-05 12 23.90	2E 792	Seyfert 1	6.67e-26
0862980101-10	0,26	03 33 49.34	-04 58 43.70	Unknown	Unknown	3.02e-6
0862980101-39	0,26	03 32 55.72	-04 56 44.40	Unknown	Unknown	4.21e-7
0863090101-9	0,84	10 07 09.27	+21 15 21.94	J100709.27+211521.9	QSO	5.41e-6
0863090101-22	0,16	10 07 36.52	+21 16 09.90	Unknown	Unknown	3.26e-5
0863710201-1	2,18	08 39 44.08	+20 36 26.32	J08394408+2036263	Star	1.19e-6
0863780101-2	0,22	11 28 53.41	+18 55 40.16	J112853.41+185540.1	QSO	1.24e-6
0863780101-25	0,21	11 29 50.10	+18 47 58.50	Unknown	Unknown	1.91e-5
0863780101-32	2,94	11 30 05.13	+18 49 28.45	J113005.14+184928.4	QSO	2.83e-4
0863780101-39	0,16	11 29 46.45	+18 55 12.50	Unknown	Unknown	7.95e-5
0863780101-45	1,13	11 28 32.57	+18 42 03.60	Unknown	Unknown	2.73e-6
0863780201-1	93.83	11 29 19.98	+18 53 31.31	Unknown	Unknown	4.08e-9
0863780201-27	0,23	11 28 56.69	+18 53 57.50	Unknown	Unknown	5.50e-6
0863890201-93	0,15	13 26 19.95	-43 05 10.10	J132619.95-430510.14	X	1.51e-7
0863960101-40	1,18	14 41 33.76	-01 07 00.85	J144133.7-010701	QSO	8.36e-7

Table 3.1: Pulsating candidates. P is the probability that the pulsation has been produced by noise, the threshold for detection has been set to 1.3e-2 corresponding to  $3\sigma$ . (\*) : Gaia DR3 4783462208935149184. (<sup>†</sup>) : source observed with Prime Large Window science mode, the frame time being 48 ms.

### 3.2 Pulse profile of the candidates

We give in figure 3.1 the pulse profile in the whole energy band (0.2 to 12 keV) of each of the candidates from table 3.1. The pulse profile in soft X-rays and hard X rays can be found in appendix.

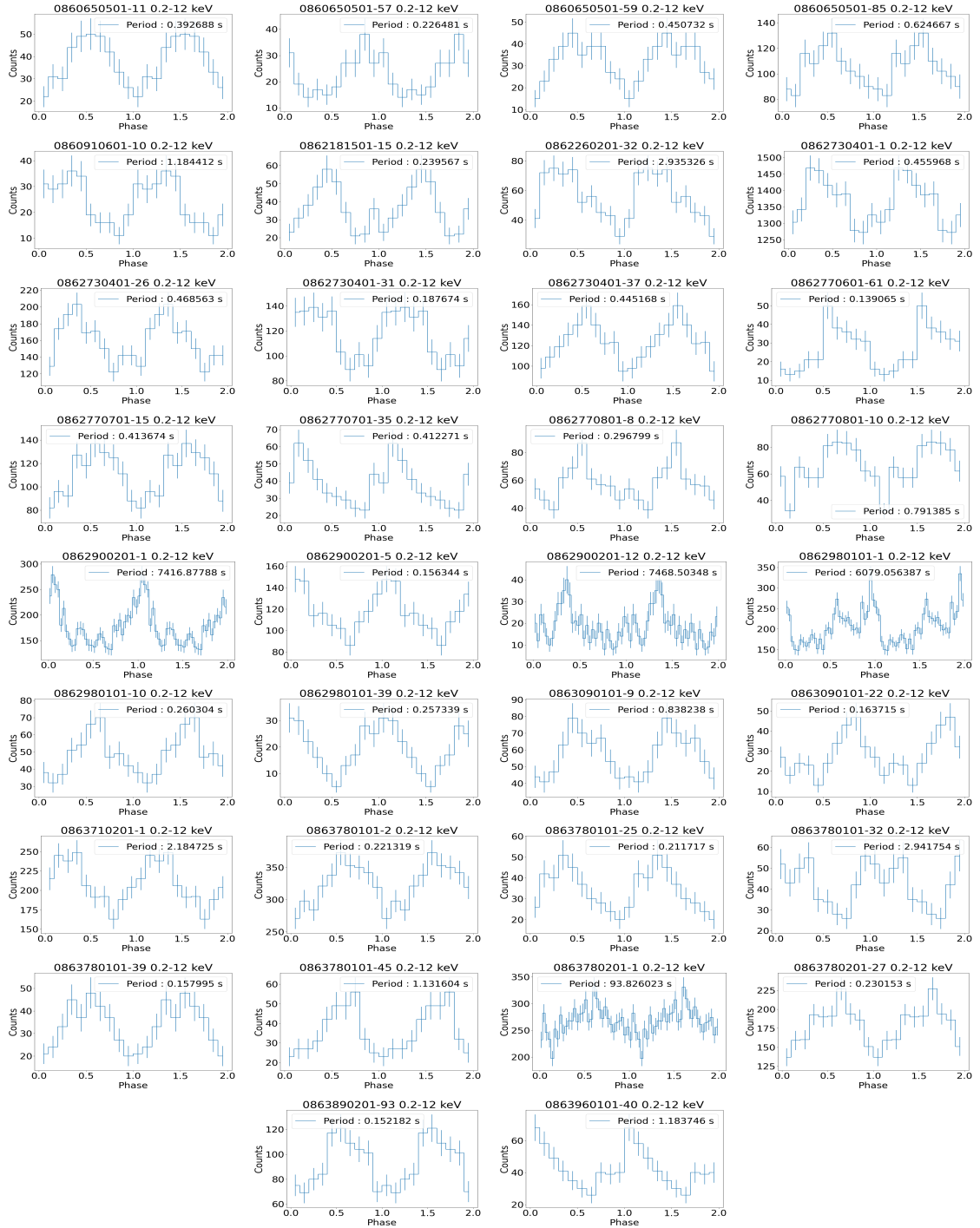


Figure 3.1: Pulse profile of the candidates from table 3.1 in the 0.2-12 keV band.

### 3.3 Spectral fitting

In this section we present the result of the spectral fitting using Xspec on the unknown candidates. We give the result of an absorbed power law and an absorbed black body fitting in table 3.2.

Source obsID-src	Inferred Nature	Period s	Best Model	$\Gamma$	$kT$ keV	$N_H$ $10^{22}$ cm $^{-2}$	$f_X$ $10^{-14}$	$\frac{f_X}{f_{opt}}$	$L$ $10^{30}$ erg s $^{-1}$	$\chi^2$ /d.o.f
0860650501-11	Star	0.39	bb	-	$0.32^{+0.10}_{-0.09}$	< 0.49	2.29	4.94e-4 *	8.26	13/11
0860650501-57	HMXB	0.23	po	$1.07^{+2.55}_{-0.76}$	-	< 0.33	1.40	-	1.68	4/4
0860650501-59	XRB ?	0.45	-	-	-	-	-	-	-	-
0860650501-85	XRB ?	0.62	-	-	-	-	-	-	-	-
0862181501-15	BHXR	0.24	po+bb	2.17	1.90	0.012	9.48	1.40 °	11.3 †	5/9
0862260201-32	HMXB	2.94	po	$1.48^{+0.52}_{-0.27}$	-	< 0.1	2.09	-	2.50 †	14/16
0862730401-26	XRB ?	0.47	-	-	-	-	-	-	-	-
0862730401-31	BHXR * ★	0.19	po	$2.32^{+1.29}_{-0.82}$	-	$0.40^{+0.44}_{-0.25}$	1.80	-	2.15 †	25/33
0862730401-37	HMXB	0.45	po	$1.28^{+0.84}_{-0.50}$	-	< 0.21	1.52	0.39 °	1.82 †	31/33
0862770701-15	BHXR	0.41	po	$1.87^{+0.67}_{-0.44}$	-	< 0.18	4.50	0.68 *	5.38 †	14/18
0862770701-35	Star	0.41	po	$2.54^{+2.28}_{-0.85}$	-	< 0.26	0.48	4.51e-2 *	0.92	8/9
0862900201-12	AGN	7468.5	po	$1.96^{+2.23}_{-0.92}$	-	< 0.48	2.33	-	2.79 †	15/19
0862980101-10	HMXB	0.26	po	$1.49^{+0.65}_{-0.26}$	-	< 0.10	5.40	-	6.46 †	26/15
0862980101-39	XRB ?	0.26	-	-	-	-	-	-	-	-
0863090101-22	HMXB * ★	0.16	po	$1.29^{+0.42}_{-0.26}$	-	< 0.11	1.69	0.44 °	2.02 †	9/7
0863780101-25	XRB	0.21	bb	-	$0.88^{+0.24}_{-0.20}$	$0.80^{+0.99}_{-0.52}$	1.30	-	1.56 †	19/10
0863780101-39	Star ? * ★	0.16	bb	-	$0.39^{+0.18}_{-0.18}$	< 0.34	0.36	-	4.31 †	7/6
0863780101-45	HMXB	1.13	po	$1.33^{+1.13}_{-0.46}$	-	< 0.19	2.52	0.32 *	3.02 †	5/7
0863780201-1	CV ? - ULX ?	93.83	po	$2.50^{+0.39}_{-0.32}$	-	< 0.08	8.19	1.25 *	9.80 †	135/146
0863780201-27	BHXR	0.23	po	$2.07^{+2.33}_{-0.81}$	-	< 0.48	1.88	0.19 °	2.25 †	67/63

Table 3.2: Best fit using either a power law (po) or a black body (bb) model on the unknown sources spectra. The pulsation detected close to the Shannon limit are designated by (\*). (?) means that we need more information to confirm the source nature. (†) indicates that the luminosity has been computed using an assumed distance of 1 kpc. (\*) indicates that the optical flux have been computed using the magnitude from GAIA and (°) from SDSS. The flux  $f_X$  is the flux between 0.2 and 12 keV and is expressed in erg cm $^{-2}$  s $^{-1}$ . The nature of the source was inferred using the pulse profiles in both the soft and hard X-ray bands, the spectrum fit and the optical counterpart when available. Errors and upper limits are at 90% confidence level

We could not obtain a power law or black body fit for 0860650501-59 (6 data points), 0860650501-85 (7 data points) and 0862980101-39 (4 data points) because of the low quality of the data. Regarding 0862730401-26, no model could be fitted because of high counts in the hard X-ray band, further investigation is thus needed.

We can compute the flux in the visible band using the G magnitude from either the GAIA database or the SDSS database (Kollmeier et al., 2019).

For GAIA data, the external calibration model <sup>1</sup> gives us the equation to compute the flux density in erg cm $^{-2}$  s $^{-1}$  Hz $^{-1}$  in the AB system :

$$m_\nu = -2.5 \log f_\nu - 48.60 \quad (3.1)$$

where  $m_\nu$  is the magnitude in the GAIA G band,  $f_\nu$  is the flux in erg cm $^{-2}$  s $^{-1}$  Hz $^{-1}$  and the

---

<sup>1</sup>[https://gea.esac.esa.int/archive/documentation/GDR2/Data\\_processing/chap\\_cu5pho/sec\\_cu5pho\\_calib](https://gea.esac.esa.int/archive/documentation/GDR2/Data_processing/chap_cu5pho/sec_cu5pho_calib)

constant term,  $-48.60$ , is defined to set  $m = 0$  mag for a source  $s_0$  with  $f_{\nu,s_0} = 3.631 \times 10^{-20}$  erg cm $^{-2}$  s $^{-1}$  Hz $^{-1}$ .

For SDSS data, we can use equation 3.2 :

$$m_\nu = -2.5 \log f_\nu + 25.11 \quad (3.2)$$

where  $m_\nu$  is the magnitude in the SDSS G band,  $f_\nu$  is the flux in nanomaggy (1 nanomaggy =  $3.631 \times 10^{-29}$  erg.cm $^{-2}$ .s $^{-1}$ .Hz $^{-1}$ ) and the constant term,  $25.11$ , is the zeropoint of the magnitude scale.

In order to compare the optical and X-ray fluxes, we must integrate  $f_\nu$  over the G band of GAIA (from 330 nm to 1050 nm) or SDSS (from 3797.64 Å to 5553.04 Å) according to equation 3.3.

$$f_{opt} = \int_{\nu_{min}}^{\nu_{max}} f_\nu d\nu \approx f_\nu (\nu_{max} - \nu_{min}) \quad (3.3)$$

The ratio  $f_X/f_{opt}$  gives us information on the dominant part of the source spectrum. For instance, the maximum of emission of a star is located in the optical band, so we expect the ratio to be  $f_X/f_{opt} \ll 1$ , whereas an isolated pulsar does not emit in the optical band so we expect the ratio to be  $f_X/f_{opt} \gg 1$ .

## 3.4 Discussion

### 3.4.1 On the pulsation's origin in quasars

In table 3.1, we report the detection of pulsations in 11 known quasars with period ranging from 0.16 seconds to 7416.9 seconds. We present here the following hypothesis : an emission coming from an over-density in orbit in the accretion disk. In this scenario, using the Schwarzschild radius and Kepler's third law, we can compute an upper bound for the mass of the central object with equation 3.4.

$$a = \left( \frac{MGT^2}{4\pi^2} \right)^{1/3} > r_s = \frac{2GM}{c^2} \Rightarrow M < \frac{1}{\sqrt{32}} \frac{c^3 T}{\pi G} \quad (3.4)$$

As these quasars are known, we have information on their redshift  $z$ , ranging from 0.139 to 2.454. If we consider that they are accreting at the Eddington limit, we can compute their mass from their distance and flux according to equation 3.5.

$$L_{Edd} = \frac{4\pi GM m_p c}{\sigma_T} = 4\pi d^2 F \Rightarrow M = \frac{d^2 F \sigma_T}{G m_p c} \quad (3.5)$$

where  $d$  is the luminosity distance computed from the redshift.

We give in table 3.3 a mass estimation of the known AGNs using the two previous assumptions. If they are accreting at or near the Eddington limit, some of these AGNs would fall into the intermediate mass black hole category ( $< 10^6 M_\odot$ ). AGNs whose mass calculated with Kepler's third law is about  $10^4 M_\odot$  cannot be observed at the calculated distances as their flux (assuming Eddington accretion) would be too low for XMM-Newton to observe ( $< 1 \times 10^{-16}$  erg s $^{-1}$  cm $^{-2}$ ). As a result, the fast pulsations detected cannot come from a blob of matter orbiting the central black hole.

obsID-src	Period s	Redshift	Distance Mpc	Flux $\times 10^{-14}$ $\text{erg s}^{-1} \text{cm}^{-2}$	Mass Eddington $\times 10^6$ $M_\odot$	Mass Kepler $\times 10^4$ $M_\odot$
0860910601-10	1,18	1,05	6299,2	5,30	2,04	1,35
0862730401-1	0,46	0,18473	857,1	28,4	0,20	0,53
0862770801-8	0,3	1,918048	13652,1	4,94	8,94	0,34
0862770801-10	0,79	0,7284	4026,2	1,61	0,25	0,90
0862900201-1	7416,9	1,46639	9621,4	21,8	19,6	8480
0862900201-5	0,16	0,508675	2636,7	5,03	0,34	0,18
0862980101-1	6079	0,139	633,7	28,6	0,11	6950
0863090101-9	0,84	0,543393	2846,9	5,30	0,42	0,96
0863780101-2	0,22	0,73598	4076,6	20,7	3,33	0,25
0863780101-32	2,94	2,454	18939,1	1,67	5,83	3,36
0863960101-40	1,18	0,9	5205,3	4,00	1,05	1,35

Table 3.3: Mass calculation of the known AGNs. Mass Eddington is computed using equation 3.5 assuming accretion at the Eddington limit and Mass Kepler is the upper limit of the central object mass using equation 3.4 for a blob of matter orbiting it at the given period.

Two of the galaxies have their stellar mass measured : 0862730401-1 ( $7.0 \pm 4.0 \times 10^{10} M_\odot$ ) and 0862980101-1 ( $9.0 \pm 6.0 \times 10^{10} M_\odot$ ) (GLADE Catalog, [Dálya et al. \(2022\)](#)). As the central super massive black hole accounts for less than 1% of the total galaxy stellar mass (e.g. [Reines & Volonteri, 2015](#)), we can place an upper limit of  $7.0 \times 10^8 M_\odot$  and  $9.0 \times 10^8 M_\odot$  on their mass. These are compatible with the Eddington and Kepler masses given in table 3.3. Given the Eddington mass computed, 0862980101-1 could be an intermediate mass black hole candidate. These mass constraints were obtained assuming a Keplerian orbit, which is a simple hypothesis. Relativistic effects should be taken into account. It should also be noted that the time resolution of EPIC-PN in Full Window mode is 73 ms and even though we accounted for the Shannon criteria, some of the pulsations are close to the Shannon limit (0.146 s) questioning the legitimacy of the detection.

### 3.4.2 Distinction based on $f_X/f_{opt}$

[Tranin et al. \(2022\)](#) developed a classification method for categorizing X-ray sources into four classes : AGN, stars, X-ray binaries, and cataclysmic variables, based on their spatial, spectral, timing properties, and multiwavelength counterparts. More precisely, the ratio  $f_X/f_{opt}$  is specific to each of these X-ray sources : between 0.1 and 10 for AGNs, below  $10^{-3}$  for stars as they are especially bright in optical and infrared , and between  $10^{-3}$  and  $10^3$  for X-ray binaries because of the numerous states they can take.

As a result we can confidently say that 0860650501-11 is a star because  $f_X/f_{opt} < 10^{-3}$ . However, the origin of such a fast pulsation (0.39 s) remains unclear. Some stars are known to exhibit pulsations, like the young T-Tauri stars with a period of 0.57 to 7.4 days ([Broeg et al., 2006](#)) or Cepheids with periods of about 1 to 70 days (e.g. [Vilardell et al., 2007](#)). All of the known pulsating stars have a period much longer than the one observed.

We can also rule out isolated pulsars, as for each source we calculated the ratio  $f_X/f_{opt}$ , the X-ray emission does not strongly dominate the optical emission. However, these sources could still contain a pulsar, but in a binary system forming an X-ray binary. The neutron star could be responsible for the X-ray emission and the stellar companion would emit in the optical band. The

ratios  $f_X/f_{opt}$  computed are within the range for X-ray binaries given by [Tranin et al. \(2022\)](#).

### 3.4.3 Distinction based on the photon index $\Gamma$

Our measurements of the photon index range from 1.07 to 2.54, however the uncertainties on these measurements are high.  $\Gamma < 1$  indicates a hard X-ray source with a steep spectrum. It is often associated with highly absorbed sources, such as heavily obscured AGNs.  $1 < \Gamma < 2$  is the most common range for X-ray sources. It typically includes a variety of objects like AGNs, XRBs (both neutron star and black hole systems), and some types of supernova remnants.  $2 < \Gamma < 3$  indicates moderately hard X-ray sources and could include some low-mass X-ray binaries and AGNs in specific states. [Lin et al. \(2012\)](#) classified 4330 X-ray sources from XMM-Newton and found that AGNs have a median photon index of 1.91 with a standard deviation of 0.31 but the photon index of stars and compact object systems is much more scattered.  $\Gamma$  tends to be high ( $> 2.5$ ) for stars and low ( $< 1.0$ ) for accretion powered pulsars.

By combining the period, the photon index and the power law fit, we tentatively identify source 0862900201-12 as an AGN, where the modulation may stem from the emission from a blob of matter in the inner accretion region (see section 3.4.1). The photon index of source 0862770701-35 is high ( $2.54^{+2.28}_{-0.85}$ ) and its emission is dominated by the optical band, making it a good candidate to be a star.

Figure 1 of [Yang et al. \(2014\)](#) shows the correlation between the X-ray photon index and X-ray luminosity ratio  $l_x = L_x/L_{Edd}$  for a sample of Black Hole X-ray Binaries (BHXRBS). In these systems, the mass of the black hole is typically between  $5 M_\odot$  and  $20 M_\odot$ , giving an Eddington luminosity between  $6.15 \times 10^{38}$  and  $2.46 \times 10^{39}$  erg s $^{-1}$ . Given the X-ray luminosity we computed in table 3.2, which is about  $10^{30}$  erg s $^{-1}$ , the luminosity ratio is approximately equal to  $10^{-9}$ . For this value of luminosity ratio, it is possible that the proposed X-ray binaries are powered by black holes (which can have luminosity in this range (e.g. [Gallo et al., 2014](#); [Coriat et al., 2011](#)) and [Yang et al. \(2014\)](#) computed  $\Gamma \approx 2.07$ . As a result 0862181501-15, 0862730401-31, 0862770701-15 and 0863780201-27 could be X-ray binaries powered by a stellar mass black hole.

High-Mass X-ray binaries (HMXB) and especially BeXB exhibit hard spectra with photon indices closer to one (e.g. [Haberl & Pietsch, 2004](#); [Reig, 2011](#)). As such, 0860650501-57, 0862260201-32, 0862730401-37, 0862980101-10, 0863090101-22 and 0863780101-45 could be HMXB as both their photon index and flux ratio point towards this hypothesis. The pulsation in these systems would be coming from the neutron star : a pulsar. However, the X-ray emission from the pulsar mechanism is complicated to deduce and is discussed in section 3.4.8.

### 3.4.4 Black body emission

Three of our candidates have a spectrum which is better modeled by a black body than by a power law, namely 0860650501-11, 0863780101-25 and 0863780101-39. This kind of spectrum could be explained by emission coming from different objects. First, it could be thermal emission from a compact object, for instance, the cooling of neutron stars surface and the polar caps can produce thermal X-rays (e.g. [Vahdat et al., 2022](#)). Then, the accretion disk in some X-ray binaries can emit thermal X-rays as its inner region can reach high temperatures (e.g. [White et al., 1988](#)). Finally, in young, active and isolated stars, the X-ray emission is usually associated with high-temperature processes in the star's outer layers, such as coronal heating or magnetic activity leading to stellar flares (e.g. [Gudel, 2004](#)).

Our candidates are modeled by a black body with a temperature between  $3.71 \times 10^6$  and  $1.02 \times 10^7$  K. We categorized 0860650501-11 as a star because of its flux dominated by the optical part. GAIA indicates an effective temperature (or surface temperature) of 5453.9 K. This confirms its the categorization, and what we are seeing in X-ray is the thermal emission from its outer layer. A corona temperature of  $3.71 \times 10^6$  K and a surface temperature of 5453.9 K could indicate that it is a G-type star. Following the same reasoning, 0863780101-39 could also be deemed as a star with an outer layer temperature of  $4.53 \times 10^6$  K, however, without a surface temperature and a comparison between its X-ray and optical flux, it cannot be affirmed with certitude. 0863780101-25 is modeled by a black body with a temperature of  $1.02 \times 10^7$  K. Stars' coronae rarely reach 10 MK, but the inner regions of accretion disks in X-ray binaries can reach temperatures of 10 MK and above for black hole with masses  $\approx 10M_\odot$  or weakly magnetized neutron stars (e.g. [White et al., 1988](#)). As such, we consider 0863780101-25 to be an X-ray binary.

### 3.4.5 Sources with failed spectra fit

The candidates with failed spectra fit (0860650501-59, 0860650501-85, 0862730401-26 and 0862980101-39) show similar pulse profiles and periods to the identified X-ray binaries. As a result, we will classify them as potential X-ray binaries (XRB ? in table [3.2](#)).

### 3.4.6 Pulse Profile

Although, their shapes seem similar, some sources exhibit a secondary peak that we can interpret in terms of emission geometry or accretion processes. 0862181501-15 shows a secondary peak only in the hard band. Some of the identified pulsating sources exhibit pulsations only in the hard X-ray band (086273041-31, 086273041-37, 0862770801-10 and 0862900201-12), while others only in the soft band (086065051-85, 0860910601-10, 0862730401-1, 0863090101-9, 0863090101-22, 0863710201-1 and 0863780101-2).

An accretion-powered pulsar exhibits pulsations primarily in the soft X-ray band. This is often due to the thermal emission from the surface of the neutron star during accretion. Soft X-rays are better suited for studying the thermal emission, and these sources may not show strong pulsations in hard X-rays. 086065051-85 and 0863090101-22 were already pointed out to be X-ray binaries. With their pulsations only detected in the soft X-ray band, we can identify the compact object to be a pulsar.

For sources where the pulsation is only detected in the hard X-ray, this could be explained by a magnetar or a pulsar with emission arising from its magnetosphere (e.g [Matz et al., 1994](#)). However, the known magnetars have been found isolated and exhibit longer pulsations ( $> 1$  s) (e.g. [Xu et al., 2022](#)), leaving only the pulsar hypothesis.

### 3.4.7 Long period pulsations

Three of our candidates exhibit long duration pulsations ( $> 1000$  s), the probability P that their pulsation has been produced by noise is given in table [3.1](#) and is extremely low ( $1.93 \times 10^{-38}$ ,  $1.19 \times 10^{-10}$  and  $6.67 \times 10^{-26}$ ). As the trial pulsation is close to the total duration of the observation ( $\approx 33$  and  $\approx 40$  ks for our detection), it becomes more and more complicated to detect an actual candidate. Figure [3.2](#) gives the  $Z_n^2$  statistic as a function of the trial frequency for 0862900201-1 as an example. We notice a squared sinc peak at the zero frequency making every trial frequency having a  $Z_n^2$  statistic above the  $3 - \sigma$  detection level. However as we have set a limit to detect

only pulsations shorter than a quarter of the duration, an other peak stands out in the residuals : the one we reported in table 3.1. As the candidate is still close to the main squared sinc peak, the computed value for the probability of the peak coming from noise is biased making it complicated to quantify the probability of detection.

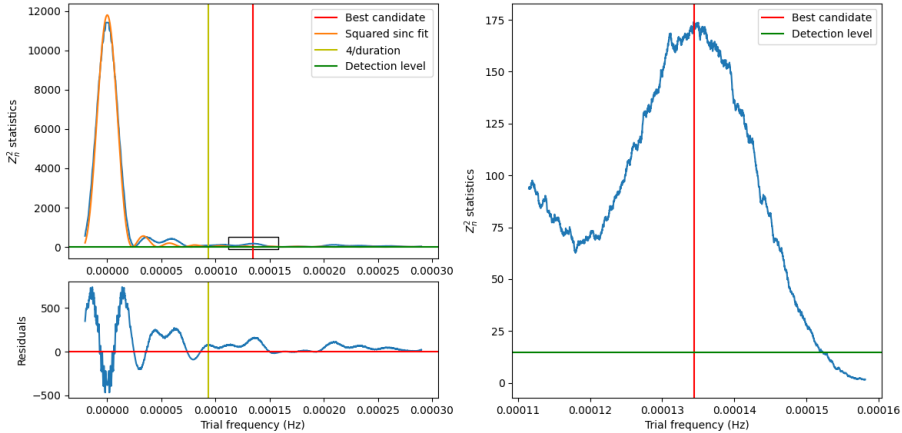


Figure 3.2: *Top left* :  $Z_n^2$  statistics in function of the trial frequency for 0862900201-1. *Bottom left* : Residuals of the squared sinc fit. *Right* : Zoom on the candidate.

As for the detection of 93.83 seconds in 0863780201-1, few pulsars, whether they are isolated or in binary systems, have been observed to pulsate in the X-ray with such a long period. Its photon index of  $2.50^{+0.39}_{-0.32}$  could indicate an X-ray binary, an AGN or a star. However its emission is dominated by the X-ray ( $f_X/f_{opt} = 1.25$ ) ruling out the star hypothesis. The only known systems to exhibit this kind of pulsation are pulsating ULXs (e.g. [Vasilopoulos et al., 2019](#)) or cataclysmic variables (e.g. [Szkody, 2021](#)). Futher investigation is needed to determine the true nature of this object.

### 3.4.8 Pulsar emission model

The Polar Cap (PC), Outer Gap (OG) and Two-pole Caustic (TPC) are three models describing the emission of a pulsar (e.g. [Venter & Harding, 2014](#)). Some of the X-ray binaries detected could contain a pulsar and the study of their X-ray pulse profiles and spectra could help to constrain the origin of the emission observed. In the PC model, X-ray emission originates from the pulsar's polar cap region as electrons are accelerated in the strong magnetic fields near the poles, producing curvature radiation and synchrotron radiation. In the OG model X-ray emission arises from a region located further out in the pulsar's magnetosphere, beyond the polar cap. Electrons and positrons are accelerated in a gap region, emitting high-energy radiation as they travel along curved magnetic field lines. In the TPC model X-ray emission is generated in regions near both magnetic poles of the pulsar. Charged particles are accelerated near both poles, and their radiation forms two beams that extend outward from the pulsar. Figure C.1 in appendix illustrate these three mechanisms.

We can spot the difference between these three models by looking at the pulse profiles for instance. [Dyks & Rudak \(2003\)](#) describes the pulse profile of pulsars in the TPC model with two peaks separated by 0.4-0.5 in phase. The peak has well developed wings and there is an inter-peak emission component. However none of the candidates' pulse profile exhibit such a pattern.

### 3.4.9 Pulsar Population

According to our previous analysis, 7 pulsars (not including the potential X-ray binaries with failed spectra fit) were discovered to emit in the X-ray from only 111 observations that are present in the XMM-Newton archive. These observations covered  $18.78^{\circ}2$  representing only 0,014% of the sky. By assuming an isotropic distribution of pulsars in the sky, there could be up to around  $5 \times 10^4$  X-ray pulsars. However, this assumption might not be realistic and the observations selected could be taken from privileged regions.

[Dirson et al. \(2022\)](#) simulates the number of observable pulsars within our Galaxy. Depending on the simulation's parameters (birth rate, initial period, initial magnetic field, ...) the total number of pulsar observable is between 489 and 16713 including radio-only, gamma-only and radio-loud gamma-ray pulsars. For pulsars observable in the X-ray band (gamma-only and radio-loud gamma-ray), this number drops between 66 and 1662. Some of their simulations are in a good agreement with the currently known pulsar population available in the Australian Telescope National Facility (ATNF) pulsar catalog ([Manchester et al., 2005](#)). This indicates that some of the pulsations attributed to pulsars in X-ray binaries might not be coming from pulsars and we need more observations to determine their nature.

# Chapter 4

## Conclusion and Perspectives

Although our analysis resulted in the detection of 34 pulsating candidates in 111 observations, we covered only a fraction of all the data available in the XMM-Newton archive : more than 15 000 observations. However, analyzing a significant part of the archive will require numerous CPU-hours as one source took up to 20 minutes on the 40 CPUs IRAP cluster to be processed. With an average of 21 sources good enough to be analyzed per observation in our sample, it will take years on the IRAP cluster to analyze the whole of the archive. The processing pipeline could be optimized to better distribute the computations on several cores, thus increasing the number of CPUs available would result in a faster computation both for the analysis pipeline and the processing pipeline.

For our analysis, we only used the EPIC-PN camera data. Its high sensitivity and time resolution were the reasons why we focused on its data. However, the other two X-ray cameras onboard of XMM-Newton, EPIC-MOS1 and EPIC-MOS2 could be used at least for spectral analysis as their spectral resolution is similar to EPIC-PN but not for timing analysis as their time resolution is worse. Integrating the insights from the three cameras could yield a more comprehensive understanding of the observed phenomena.

In the future analysis of the rest of XMM-Newton data, given the results of this study, we hope to discover new pulsating ULXs and thus constrain the number of ULXs containing neutron star compared to those containing a black hole. This would help us understand the formation and evolution of ULXs but also to understand if they are at the origin of compact binary coalescence emitting gravitational waves.

The detection of pulsations in several quasars, with periods ranging from 0.2 seconds to close to 10,000 seconds, could help us constrain the mass of supermassive black holes and identify new EMRIs and Quasi-Periodic Eruptions (QPEs). As we found some clues pointing toward a low mass AGN that could be an intermediate mass black hole, the technique used here could be a great tool to detect pulsations coming from the accretion disk around these particular black holes.

However, the origin of these X-ray pulsations in quasars remains a mystery. We suggested, that these pulsations come from a blob of matter in the inner accretion disk. They cannot come from an pulsating source orbiting the black hole because it will be too faint at such distances. While long periods can be explained by the over-density in the accretion disk, fast pulsations lead to central black holes with masses too small to be observed. Further investigation is needed to distinguish between these possibilities. If confirmed as pulsating objects, this could signify the presence of exotic companions such as neutron stars or white dwarfs in close proximity to the black holes.

More X-ray observations of the pulsating candidates are needed in the future in order to rule

out a transient behavior. Additionally, multi-wavelength observations could also help us determine their nature. The detection of pulsations in the radio band would provide evidence of a neutron star and confirm its rotational period, which may be linked to the observed X-ray pulsations. Optical and infrared observations, could reveal the presence of stars or white dwarfs close to the black hole.

## References

- Amaro-Seoane, P. 2018, Living Reviews in Relativity, 21, doi: [10.1007/s41114-018-0013-8](https://doi.org/10.1007/s41114-018-0013-8)
- Amaro-Seoane, P., Gair, J. R., Freitag, M., et al. 2007, Classical and Quantum Gravity, 24, R113, doi: [10.1088/0264-9381/24/17/R01](https://doi.org/10.1088/0264-9381/24/17/R01)
- Amaro-Seoane, P., Audley, H., Babak, S., et al. 2017, arXiv e-prints, arXiv:1702.00786, doi: [10.48550/arXiv.1702.00786](https://doi.org/10.48550/arXiv.1702.00786)
- Andersen, B. C., & Ransom, S. M. 2018, The Astrophysical Journal, 863, L13, doi: [10.3847/2041-8213/aad59f](https://doi.org/10.3847/2041-8213/aad59f)
- Arnaud, K. A. 1996, 101, 17
- Arviset, C., Guainazzi, M., Hernandez, J., et al. 2002, arXiv e-prints, astro, doi: [10.48550/arXiv.astro-ph/0206412](https://doi.org/10.48550/arXiv.astro-ph/0206412)
- Bachetti, M. 2018, HENDRICS: High ENergy Data Reduction Interface from the Command Shell, Astrophysics Source Code Library, record ascl:1805.019. <http://ascl.net/1805.019>
- Bachetti, M., & Huppenkothen, D. 2022, Fourier Domain, arXiv, doi: [10.48550/ARXIV.2209.07954](https://doi.org/10.48550/ARXIV.2209.07954)
- Bachetti, M., Harrison, F. A., Walton, D. J., et al. 2014, Nature, 514, 202, doi: [10.1038/nature13791](https://doi.org/10.1038/nature13791)
- Bachetti, M., Huppenkothen, D., Khan, U., et al. 2022, StingraySoftware/stingray: v1.1, v1.1, Zenodo, doi: [10.5281/zenodo.7135161](https://doi.org/10.5281/zenodo.7135161)
- Basu, J. K. 2014, Resonance, 19, 1158, doi: [10.1007/s12045-014-0140-9](https://doi.org/10.1007/s12045-014-0140-9)
- Belczynski, K., & Taam, R. E. 2008, The Astrophysical Journal, 685, 400, doi: [10.1086/590551](https://doi.org/10.1086/590551)
- Bernadich, M. C., Schworer, A. D., Kovlakas, K., Zezas, A., & Traulsen, I. 2022, Astronomy & Astrophysics, 659, A188, doi: [10.1051/0004-6361/202141560](https://doi.org/10.1051/0004-6361/202141560)
- Beskin, V. S., Chernov, S. V., Gwinn, C. R., & Tchekhovskoy, A. A. 2015, Space Science Reviews, 191, 207, doi: [10.1007/s11214-015-0173-8](https://doi.org/10.1007/s11214-015-0173-8)
- Boissay, R., Ricci, C., & Paltani, S. 2016, Astronomy & Astrophysics, 588, A70, doi: [10.1051/0004-6361/201526982](https://doi.org/10.1051/0004-6361/201526982)
- Bowyer, S., Byram, E. T., Chubb, T. A., & Friedman, H. 1964, Nature, 201, 1307, doi: [10.1038/2011307a0](https://doi.org/10.1038/2011307a0)
- Brice, N., Zane, S., Turolla, R., & Wu, K. 2021, Monthly Notices of the Royal Astronomical Society, 504, 701, doi: [10.1093/mnras/stab915](https://doi.org/10.1093/mnras/stab915)
- Broeg, C., Joergens, V., Fernández, M., et al. 2006, Astronomy & Astrophysics, 450, 1135, doi: [10.1051/0004-6361:20053777](https://doi.org/10.1051/0004-6361:20053777)
- Buccheri, R., Bennett, K., Bignami, G. F., et al. 1983, , 128, 245
- Burrows, D. N., Hill, J. E., Nosek, J. A., et al. 2005, , 120, 165, doi: [10.1007/s11214-005-5097-2](https://doi.org/10.1007/s11214-005-5097-2)
- Cameron, A. D., Barr, E. D., Champion, D. J., Kramer, M., & Zhu, W. W. 2017, Monthly Notices of the Royal Astronomical Society, 468, 1994, doi: [10.1093/mnras/stx589](https://doi.org/10.1093/mnras/stx589)

- Cassam-Chenai, G., Decourchelle, A., Ballet, J., et al. 2004, *Astronomy & Astrophysics*, 427, 199, doi: [10.1051/0004-6361:20041154](https://doi.org/10.1051/0004-6361:20041154)
- Chen, R.-C., Deng, C.-M., Wang, X.-G., et al. 2023, *Research in Astronomy and Astrophysics*, 23, 085018, doi: [10.1088/1674-4527/acdbe](https://doi.org/10.1088/1674-4527/acdbe)
- Collazos, J. A. 2023, Structural characteristics and physical properties of neutron stars: theoretical and observational research. <https://arxiv.org/abs/2303.08734>
- Coriat, M., Corbel, S., Prat, L., et al. 2011, *Monthly Notices of the Royal Astronomical Society*, 414, 677, doi: [10.1111/j.1365-2966.2011.18433.x](https://doi.org/10.1111/j.1365-2966.2011.18433.x)
- Corral, A., Ceca, R. D., Caccianiga, A., et al. 2011, *Astronomy & Astrophysics*, 530, A42, doi: [10.1051/0004-6361/201015227](https://doi.org/10.1051/0004-6361/201015227)
- Dálya, G., Díaz, R., Bouchet, F. R., et al. 2022, *Monthly Notices of the Royal Astronomical Society*, 514, 1403, doi: [10.1093/mnras/stac1443](https://doi.org/10.1093/mnras/stac1443)
- de Jager, O. C., & Büsching, I. 2010, *Astronomy and Astrophysics*, 517, L9, doi: [10.1051/0004-6361/201014362](https://doi.org/10.1051/0004-6361/201014362)
- den Herder, J. W., Brinkman, A. C., Kahn, S. M., et al. 2001, *Astronomy & Astrophysics*, 365, L7, doi: [10.1051/0004-6361:20000058](https://doi.org/10.1051/0004-6361:20000058)
- Dickey, J. M., & Lockman, F. J. 1990, , 28, 215, doi: [10.1146/annurev.aa.28.090190.001243](https://doi.org/10.1146/annurev.aa.28.090190.001243)
- Dimoudi, S., Adamek, K., Thiagaraj, P., et al. 2018, *The Astrophysical Journal Supplement Series*, 239, 28, doi: [10.3847/1538-4365/aabe88](https://doi.org/10.3847/1538-4365/aabe88)
- Dirson, L., Pétri, J., & Mitra, D. 2022, *Astronomy & Astrophysics*, 667, A82, doi: [10.1051/0004-6361/202243305](https://doi.org/10.1051/0004-6361/202243305)
- Dyks, J., & Rudak, B. 2003, , 598, 1201, doi: [10.1086/379052](https://doi.org/10.1086/379052)
- Ebrero, J. 2023. [http://xmm-tools.cosmos.esa.int/external/xmm\\_user\\_support/documentation/uhb/XMM\\_UHB.pdf](http://xmm-tools.cosmos.esa.int/external/xmm_user_support/documentation/uhb/XMM_UHB.pdf)
- Ellison, S. L., Wilkinson, S., Woo, J., et al. 2022, *Monthly Notices of the Royal Astronomical Society: Letters*, 517, L92, doi: [10.1093/mnrasl/slac109](https://doi.org/10.1093/mnrasl/slac109)
- Fabian, A. C. 1999, *Proceedings of the National Academy of Sciences*, 96, 4749, doi: [10.1073/pnas.96.9.4749](https://doi.org/10.1073/pnas.96.9.4749)
- Foord, A., Liu, X., Gültekin, K., et al. 2022, , 927, 3, doi: [10.3847/1538-4357/ac4af1](https://doi.org/10.3847/1538-4357/ac4af1)
- Fragkos, A. 2011
- Frank, J., King, A., & Raine, D. J. 2002, *Accretion Power in Astrophysics*: Third Edition
- Fryer, C. L. 1999, *The Astrophysical Journal*, 522, 413, doi: [10.1086/307647](https://doi.org/10.1086/307647)
- Gabriel, C., Denby, M., Fyfe, D. J., et al. 2004, 314, 759
- Gaia Collaboration, Prusti, T., de Bruijne, J. H. J., et al. 2016, , 595, A1, doi: [10.1051/0004-6361/201629272](https://doi.org/10.1051/0004-6361/201629272)
- Gaia Collaboration, Vallenari, A., Brown, A. G. A., et al. 2023, , 674, A1, doi: [10.1051/0004-6361/202243940](https://doi.org/10.1051/0004-6361/202243940)
- Gallo, E., Miller-Jones, J. C. A., Russell, D. M., et al. 2014, *Monthly Notices of the Royal Astronomical Society*, 445, 290, doi: [10.1093/mnras/stu1599](https://doi.org/10.1093/mnras/stu1599)
- Gallo, L. C., Miller, J. M., & Costantini, E. 2023, Active galactic nuclei with high-resolution X-ray spectroscopy, arXiv, doi: [10.48550/ARXIV.2302.10930](https://doi.org/10.48550/ARXIV.2302.10930)
- Ghosh, T., & Rana, V. 2023, *The Astrophysical Journal*, 949, 78, doi: [10.3847/1538-4357/acccf4](https://doi.org/10.3847/1538-4357/acccf4)
- Giacconi, R., Gursky, H., Paolini, F. R., & Rossi, B. B. 1962, *Phys. Rev. Lett.*, 9, 439, doi: [10.1103/PhysRevLett.9.439](https://doi.org/10.1103/PhysRevLett.9.439)

- Gibson, A. I., Harrison, A. B., Kirkman, I. W., et al. 1982, *Nature*, 296, 833, doi: [10.1038/296833a0](https://doi.org/10.1038/296833a0)
- Göhler, E., Wilms, J., & Staubert, R. 2005, *Astronomy & Astrophysics*, 433, 1079, doi: [10.1051/0004-6361:20042101](https://doi.org/10.1051/0004-6361:20042101)
- Grupe, D., Gronwall, C., Wang, X.-Y., et al. 2007, *The Astrophysical Journal*, 662, 443, doi: [10.1086/517868](https://doi.org/10.1086/517868)
- Gudel, M. 2004, *The Astronomy and Astrophysics Review*, 12, doi: [10.1007/s00159-004-0023-2](https://doi.org/10.1007/s00159-004-0023-2)
- Haberl, F., & Pietsch, W. 2004, *Astronomy & Astrophysics*, 414, 667, doi: [10.1051/0004-6361:20031654](https://doi.org/10.1051/0004-6361:20031654)
- Hameury, J.-M., & Lasota, J.-P. 2020, *Astronomy & Astrophysics*, 643, A171, doi: [10.1051/0004-6361/202038857](https://doi.org/10.1051/0004-6361/202038857)
- Harrison, F. A., Craig, W. W., Christensen, F. E., et al. 2013, *The Astrophysical Journal*, 770, 103, doi: [10.1088/0004-637x/770/2/103](https://doi.org/10.1088/0004-637x/770/2/103)
- Hewish, A., Bell, S. J., Pilkington, J. D. H., Scott, P. F., & Collins, R. A. 1968, *Nature*, 217, 709, doi: [10.1038/217709a0](https://doi.org/10.1038/217709a0)
- Hobbs, G., & Dai, S. 2017, *National Science Review*, 4, 707, doi: [10.1093/nsr/nwx126](https://doi.org/10.1093/nsr/nwx126)
- Huppenkothen, D., Bachetti, M., Stevens, A., et al. 2019, *Journal of Open Source Software*, 4, 1393, doi: [10.21105/joss.01393](https://doi.org/10.21105/joss.01393)
- Huppenkothen, D., Bachetti, M., Stevens, A. L., et al. 2019, *apj*, 881, 39, doi: [10.3847/1538-4357/ab258d](https://doi.org/10.3847/1538-4357/ab258d)
- Iben, I. 1974, *Annual Review of Astronomy and Astrophysics*, 12, 215, doi: [10.1146/annurev.aa.12.090174.001243](https://doi.org/10.1146/annurev.aa.12.090174.001243)
- Igoshev, A. P., Popov, S. B., & Hollerbach, R. 2021, Evolution of neutron star magnetic fields. <https://arxiv.org/abs/2109.05584>
- Jain, C., & Paul, B. 2011, *Research in Astronomy and Astrophysics*, 11, 1134, doi: [10.1088/1674-4527/11/10/002](https://doi.org/10.1088/1674-4527/11/10/002)
- Jansen, F., Lumb, D., Altieri, B., et al. 2001, *Astronomy & Astrophysics*, 365, L1, doi: [10.1051/0004-6361:20000036](https://doi.org/10.1051/0004-6361:20000036)
- Johnston, H. M., & Kulkarni, S. R. 1991, , 368, 504, doi: [10.1086/169715](https://doi.org/10.1086/169715)
- Johnston, S., & Karastergiou, A. 2017, *Monthly Notices of the Royal Astronomical Society*, 467, 3493, doi: [10.1093/mnras/stx377](https://doi.org/10.1093/mnras/stx377)
- Kaspi, V. M., & Beloborodov, A. 2017, doi: [10.48550/ARXIV.1703.00068](https://doi.org/10.48550/ARXIV.1703.00068)
- Kimpson, T., Wu, K., & Zane, S. 2019, *Monthly Notices of the Royal Astronomical Society*, 486, 360, doi: [10.1093/mnras/stz845](https://doi.org/10.1093/mnras/stz845)
- Koester, D. 2013, in *Planets, Stars and Stellar Systems* (Springer Netherlands), 559–612, doi: [10.1007/978-94-007-5615-1\\_11](https://doi.org/10.1007/978-94-007-5615-1_11)
- Kollmeier, J., Anderson, S. F., Blanc, G. A., et al. 2019, in *Bulletin of the American Astronomical Society*, Vol. 51, 274
- Kouveliotou, C., Meegan, C. A., Fishman, G. J., et al. 1993, , 413, L101, doi: [10.1086/186969](https://doi.org/10.1086/186969)
- Kramer, M., Stairs, I., Manchester, R., et al. 2021, *Physical Review X*, 11, doi: [10.1103/physrevx.11.041050](https://doi.org/10.1103/physrevx.11.041050)
- Kunitomo, M., Guillot, T., Takeuchi, T., & Ida, S. 2017, *Astronomy & Astrophysics*, 599, A49, doi: [10.1051/0004-6361/201628260](https://doi.org/10.1051/0004-6361/201628260)
- Lattimer, J. M., & Prakash, M. 2004, *Science*, 304, 536, doi: [10.1126/science.1090720](https://doi.org/10.1126/science.1090720)
- Lazarus, P., Brazier, A., Hessels, J. W. T., et al. 2015, , 812, 81, doi: [10.1088/0004-637X/812/1/81](https://doi.org/10.1088/0004-637X/812/1/81)
- Leahy, D. A., Darbro, W., Elsner, R. F., et al. 1983, *The Astrophysical Journal*, 266, 160, doi: [10.1086/160766](https://doi.org/10.1086/160766)

- Lin, D., Webb, N. A., & Barret, D. 2012, The Astrophysical Journal, 756, 27, doi: [10.1088/0004-637x/756/1/27](https://doi.org/10.1088/0004-637x/756/1/27)
- Lin, D. N. C., Papaloizou, J., & Faulkner, J. 1985, Monthly Notices of the Royal Astronomical Society, 212, 105, doi: [10.1093/mnras/212.1.105](https://doi.org/10.1093/mnras/212.1.105)
- Lomb, N. R. 1976, *Astrophysics and Space Science*, 39, 447, doi: [10.1007/bf00648343](https://doi.org/10.1007/bf00648343)
- Lorimer, D. R., & Kramer, M. 2004, *Handbook of Pulsar Astronomy*, Vol. 4
- Lyne, A. G., Pritchard, R. S., & Shemar, S. L. 1995, *Journal of Astrophysics and Astronomy*, 16, 179, doi: [10.1007/bf02714833](https://doi.org/10.1007/bf02714833)
- Lyne, A. G., Shemar, S. L., & Smith, F. G. 2000, *Monthly Notices of the Royal Astronomical Society*, 315, 534, doi: [10.1046/j.1365-8711.2000.03415.x](https://doi.org/10.1046/j.1365-8711.2000.03415.x)
- MacKenzie, A. D. A., Roberts, T. P., & Walton, D. J. 2023, *Astronomische Nachrichten*, 344, doi: [10.1002/asna.20230028](https://doi.org/10.1002/asna.20230028)
- Maiorano, M., Paolis, F. D., & Nucita, A. A. 2021, *Symmetry*, 13, 2418, doi: [10.3390/sym13122418](https://doi.org/10.3390/sym13122418)
- Manchester, R. N. 2017, *Journal of Physics: Conference Series*, 932, 012002, doi: [10.1088/1742-6596/932/1/012002](https://doi.org/10.1088/1742-6596/932/1/012002)
- Manchester, R. N., Hobbs, G. B., Teoh, A., & Hobbs, M. 2005, , 129, 1993, doi: [10.1086/428488](https://doi.org/10.1086/428488)
- Mardia, K. V. 1975, *Journal of the Royal Statistical Society: Series B (Methodological)*, 37, 349, doi: [10.1111/j.2517-6161.1975.tb01550.x](https://doi.org/10.1111/j.2517-6161.1975.tb01550.x)
- Marsh, T. R., Gänsicke, B. T., Hümmerich, S., et al. 2016, *Nature*, 537, 374, doi: [10.1038/nature18620](https://doi.org/10.1038/nature18620)
- Mason, K. O., Breeveld, A., Much, R., et al. 2001, *Astronomy & Astrophysics*, 365, L36, doi: [10.1051/0004-6361:20000044](https://doi.org/10.1051/0004-6361:20000044)
- Matz, S., Ulmer, M. P., Grabelsky, D. A., et al. 1994, *The Astrophysical Journal*, 434, 288, doi: [10.1086/174727](https://doi.org/10.1086/174727)
- McCrory, R., & Hatchett, S. 1975, , 199, 196, doi: [10.1086/153681](https://doi.org/10.1086/153681)
- McWilliams, S. T., Ostriker, J. P., & Pretorius, F. 2014, *The Astrophysical Journal*, 789, 156, doi: [10.1088/0004-637x/789/2/156](https://doi.org/10.1088/0004-637x/789/2/156)
- Mereghetti, S., Tiengo, A., & Esposito, P. 2008, *Astronomische Nachrichten*, 329, 194, doi: [10.1002/asna.200710911](https://doi.org/10.1002/asna.200710911)
- Mereghetti, S., Tiengo, A., Esposito, P., et al. 2005, *The Astrophysical Journal*, 628, 938, doi: [10.1086/430943](https://doi.org/10.1086/430943)
- Metzger, B. D., Stone, N. C., & Gilbaum, S. 2022, *The Astrophysical Journal*, 926, 101, doi: [10.3847/1538-4357/ac3ee1](https://doi.org/10.3847/1538-4357/ac3ee1)
- Middleditch, J., Deich, W., & Kulkarni, S. 1993, in *Isolated Pulsars*, ed. K. A. van Riper, R. I. Epstein, & C. Ho, 372
- Mineo, S., Gilfanov, M., & Sunyaev, R. 2011, *Monthly Notices of the Royal Astronomical Society*, 419, 2095, doi: [10.1111/j.1365-2966.2011.19862.x](https://doi.org/10.1111/j.1365-2966.2011.19862.x)
- Misra, D., Fragos, T., Tauris, T. M., Zapartas, E., & Aguilera-Dena, D. R. 2020, *Astronomy & Astrophysics*, 642, A174, doi: [10.1051/0004-6361/202038070](https://doi.org/10.1051/0004-6361/202038070)
- Moore, C. J., Chua, A. J. K., & Gair, J. R. 2017, *Classical and Quantum Gravity*, 34, 195009, doi: [10.1088/1361-6382/aa85fa](https://doi.org/10.1088/1361-6382/aa85fa)
- Murray, S., et al. 2009. <https://arxiv.org/abs/0903.5272>
- Mushtukov, A. A., Zwart, S. P., Tsygankov, S. S., Nagirner, D. I., & Poutanen, J. 2020, *Monthly Notices of the Royal Astronomical Society*, 501, 2424, doi: [10.1093/mnras/staa3809](https://doi.org/10.1093/mnras/staa3809)

- Nagase, F. 1989, , 41, 1
- Ochsenbein, F. 1996, The VizieR database of astronomical catalogues, CDS, Centre de Données astronomiques de Strasbourg, doi: [10.26093/CDS/VIZIER](https://doi.org/10.26093/CDS/VIZIER)
- Okun, L. B., Selivanov, K. G., & Teleghi, V. L. 2000, American Journal of Physics, 68, 115, doi: [10.1119/1.19382](https://doi.org/10.1119/1.19382)
- Padovani, P., Alexander, D. M., Assef, R. J., et al. 2017, The Astronomy and Astrophysics Review, 25, doi: [10.1007/s00159-017-0102-9](https://doi.org/10.1007/s00159-017-0102-9)
- Papitto, A., Ferrigno, C., Bozzo, E., et al. 2013, Nature, 501, 517, doi: [10.1038/nature12470](https://doi.org/10.1038/nature12470)
- Pareschi, G., Spiga, D., & Pelliciari, C. 2021, in The WSPC Handbook of Astronomical Instrumentation (WORLD SCIENTIFIC), 3–31, doi: [10.1142/9789811203800\\_0001](https://doi.org/10.1142/9789811203800_0001)
- Peacock, M. B., Zepf, S. E., Maccarone, T. J., et al. 2014, The Astrophysical Journal, 784, 162, doi: [10.1088/0004-637x/784/2/162](https://doi.org/10.1088/0004-637x/784/2/162)
- Pearlman, A. B., Coley, J. B., Corbet, R. H. D., & Pottschmidt, K. 2019, The Astrophysical Journal, 873, 86, doi: [10.3847/1538-4357/aaf001](https://doi.org/10.3847/1538-4357/aaf001)
- Pelisoli, I., Marsh, T. R., Buckley, D. A. H., et al. 2023, A 5.3-minute-period pulsing white dwarf in a binary detected from radio to X-rays, arXiv, doi: [10.48550/ARXIV.2306.09272](https://doi.org/10.48550/ARXIV.2306.09272)
- Phinney, E. S. 1992, Philosophical Transactions: Physical Sciences and Engineering, 341, 39. <http://www.jstor.org/stable/53911>
- Piran, T., Bromberg, O., Nakar, E., & Sari, R. 2013, Philosophical Transactions of the Royal Society A: Mathematical, Physical and Engineering Sciences, 371, 20120273, doi: [10.1098/rsta.2012.0273](https://doi.org/10.1098/rsta.2012.0273)
- Podsiadlowski, P., Rappaport, S., & Pfahl, E. D. 2002, The Astrophysical Journal, 565, 1107, doi: [10.1086/324686](https://doi.org/10.1086/324686)
- Quintin, E., Webb, N. A., Gúrpide, A., Bachetti, M., & Fürst, F. 2021, Monthly Notices of the Royal Astronomical Society, 503, 5485, doi: [10.1093/mnras/stab814](https://doi.org/10.1093/mnras/stab814)
- Ramsey, B. D., Austin, R. A., & Decher, R. 1993, Instrumentation for x-ray astronomy, Technical Report, NASA Marshall Space Flight Center Huntsville, AL United States
- Ransom, S. M., Eikenberry, S. S., & Middleitch, J. 2002, , 124, 1788, doi: [10.1086/342285](https://doi.org/10.1086/342285)
- Reig, P. 2011, Astrophysics and Space Science, 332, 1, doi: [10.1007/s10509-010-0575-8](https://doi.org/10.1007/s10509-010-0575-8)
- Reines, A. E., & Volonteri, M. 2015, The Astrophysical Journal, 813, 82, doi: [10.1088/0004-637x/813/2/82](https://doi.org/10.1088/0004-637x/813/2/82)
- Salvo, T. D., & Sanna, A. 2021, in Astrophysics and Space Science Library (Springer International Publishing), 87–124, doi: [10.1007/978-3-030-85198-9\\_4](https://doi.org/10.1007/978-3-030-85198-9_4)
- Sasaki, M., Müller, D., Kraus, U., Ferrigno, C., & Santangelo, A. 2012, Astronomy & Astrophysics, 540, A35, doi: [10.1051/0004-6361/201016304](https://doi.org/10.1051/0004-6361/201016304)
- Scargle, J. D. 1982, The Astrophysical Journal, 263, 835, doi: [10.1086/160554](https://doi.org/10.1086/160554)
- Schröder, C., Hubrig, S., & Schmitt, J. H. M. M. 2008, Astronomy & Astrophysics, 484, 479, doi: [10.1051/0004-6361:20078963](https://doi.org/10.1051/0004-6361:20078963)
- Schwpo, A., Marsh, T. R., Standke, A., et al. 2023, , 674, L9, doi: [10.1051/0004-6361/202346589](https://doi.org/10.1051/0004-6361/202346589)
- Smith, R. C. 2007, Cataclysmic Variables, arXiv, doi: [10.48550/ARXIV.ASTRO-PH/0701654](https://doi.org/10.48550/ARXIV.ASTRO-PH/0701654)
- Southworth, J., Copperwheat, C. M., Gänsicke, B. T., & Pyrzas, S. 2010, Astronomy and Astrophysics, 510, A100, doi: [10.1051/0004-6361/200913576](https://doi.org/10.1051/0004-6361/200913576)
- Steeghs, D., & Casares, J. 2002, The Astrophysical Journal, 568, 273, doi: [10.1086/339224](https://doi.org/10.1086/339224)

- Suh, I.-S., & Mathews, G. J. 2010, The Astrophysical Journal, 717, 843, doi: [10.1088/0004-637x/717/2/843](https://doi.org/10.1088/0004-637x/717/2/843)
- Szkody, P. 2021, Frontiers in Astronomy and Space Sciences, 8, doi: [10.3389/fspas.2021.759686](https://doi.org/10.3389/fspas.2021.759686)
- Tadhunter, C. 2008, New Astronomy Reviews, 52, 227, doi: [10.1016/j.newar.2008.06.004](https://doi.org/10.1016/j.newar.2008.06.004)
- Takata, J., Hu, C.-P., Lin, L. C. C., et al. 2018, The Astrophysical Journal, 853, 106, doi: [10.3847/1538-4357/aaa23d](https://doi.org/10.3847/1538-4357/aaa23d)
- Tam, S.-I., Jauzac, M., Massey, R., et al. 2020, Monthly Notices of the Royal Astronomical Society, 496, 4032, doi: [10.1093/mnras/staa1828](https://doi.org/10.1093/mnras/staa1828)
- Tan, C. 2021, Journal of Physics: Conference Series, 2012, 012119, doi: [10.1088/1742-6596/2012/1/012119](https://doi.org/10.1088/1742-6596/2012/1/012119)
- Tauris, T. M., van den Heuvel, E. P. J., & Savonije, G. J. 2000, , 530, L93, doi: [10.1086/312496](https://doi.org/10.1086/312496)
- Testa, P. 2010, Proceedings of the National Academy of Sciences, 107, 7158, doi: [10.1073/pnas.0913822107](https://doi.org/10.1073/pnas.0913822107)
- Testa, P., Saar, S. H., & Drake, J. J. 2015, Philosophical Transactions of the Royal Society A: Mathematical, Physical and Engineering Sciences, 373, 20140259, doi: [10.1098/rsta.2014.0259](https://doi.org/10.1098/rsta.2014.0259)
- Townsend, L. J., Coe, M. J., Corbet, R. H. D., & Hill, A. B. 2011, Monthly Notices of the Royal Astronomical Society, 416, 1556, doi: [10.1111/j.1365-2966.2011.19153.x](https://doi.org/10.1111/j.1365-2966.2011.19153.x)
- Tranin, H., Godet, O., Webb, N., & Primorac, D. 2022, Astronomy & Astrophysics, 657, A138, doi: [10.1051/0004-6361/202141259](https://doi.org/10.1051/0004-6361/202141259)
- Turner, M. J. L., Arnaud, M., Reppin, C., & Villa, G. 1998, 191, 96.04
- Turner, M. J. L., Abbey, A., Arnaud, M., et al. 2001, Astronomy & Astrophysics, 365, L27, doi: [10.1051/0004-6361:20000087](https://doi.org/10.1051/0004-6361:20000087)
- Vahdat, A., Posselt, B., Santangelo, A., & Pavlov, G. G. 2022, Astronomy & Astrophysics, 658, A95, doi: [10.1051/0004-6361/202141795](https://doi.org/10.1051/0004-6361/202141795)
- Vasilopoulos, G., Petropoulou, M., Koliopanos, F., et al. 2019, Monthly Notices of the Royal Astronomical Society, 488, 5225, doi: [10.1093/mnras/stz2045](https://doi.org/10.1093/mnras/stz2045)
- Venter, C., & Harding, A. 2014, Astronomische Nachrichten, 335, 268, doi: [10.1002/asna.201312030](https://doi.org/10.1002/asna.201312030)
- Verbunt, F., & Rappaport, S. A. 1988, The Astrophysical Journal, 332, 193. <https://api.semanticscholar.org/CorpusID:120663036>
- Vidana, I. 2018, doi: [10.48550/ARXIV.1805.00837](https://doi.org/10.48550/ARXIV.1805.00837)
- Vilardell, F., Jordi, C., & Ribas, I. 2007, Astronomy & Astrophysics, 473, 847, doi: [10.1051/0004-6361:200777960](https://doi.org/10.1051/0004-6361:200777960)
- Walton, D. J., Mackenzie, A. D. A., Gully, H., et al. 2021, Monthly Notices of the Royal Astronomical Society, 509, 1587, doi: [10.1093/mnras/stab3001](https://doi.org/10.1093/mnras/stab3001)
- Wang, Y., ZHENG, W., ZHANG, S., et al. 2023, Chinese Journal of Aeronautics, doi: [10.1016/j.cja.2023.03.002](https://doi.org/10.1016/j.cja.2023.03.002)
- Watson, M. G., Auguères, J. L., Ballet, J., et al. 2001, , 365, L51, doi: [10.1051/0004-6361:20000067](https://doi.org/10.1051/0004-6361:20000067)
- Weisskopf, M. C., Tananbaum, H. D., Speybroeck, L. P. V., & O'Dell, S. L. 2000, in SPIE Proceedings, ed. J. E. Truemper & B. Aschenbach (SPIE), doi: [10.1117/12.391545](https://doi.org/10.1117/12.391545)
- Welch, P. 1967, IEEE Transactions on Audio and Electroacoustics, 15, 70, doi: [10.1109/tau.1967.1161901](https://doi.org/10.1109/tau.1967.1161901)

- Wenger, M., Ochsenbein, F., Egret, D., et al. 2000, , 143, 9, doi: [10.1051/aas:2000332](https://doi.org/10.1051/aas:2000332)
- White, N., Stella, L., & Parmar, A. 1988, , 324, 363, doi: [10.1086/165901](https://doi.org/10.1086/165901)
- Wilkes, B. J., Tucker, W., Schartel, N., & Santos-Lleo, M. 2022, Nature, 606, 261, doi: [10.1038/s41586-022-04481-y](https://doi.org/10.1038/s41586-022-04481-y)
- Wilson, R. N. 1996, Reflecting Telescope Optics I. Basic Design Theory and its Historical Development.
- Wolter, H. 1952, Annalen der Physik, 445, 286, doi: <https://doi.org/10.1002/andp.19524450410>
- Xu, K., Li, X.-D., Cui, Z., et al. 2022, Research in Astronomy and Astrophysics, 22, 015005, doi: [10.1088/1674-4527/ac321f](https://doi.org/10.1088/1674-4527/ac321f)
- Yang, Q.-X., Xie, F.-G., Yuan, F., et al. 2014, Monthly Notices of the Royal Astronomical Society, 447, 1692, doi: [10.1093/mnras/stu2571](https://doi.org/10.1093/mnras/stu2571)
- Yue-zhu, Z., Yan-yan, F., Yi-huan, W., et al. 2016, Chinese Astronomy and Astrophysics, 40, 210, doi: [10.1016/j.chinastron.2016.05.001](https://doi.org/10.1016/j.chinastron.2016.05.001)
- Zakhzhay, V. A. 2013, Kinematics and Physics of Celestial Bodies, 29, 195, doi: [10.3103/s0884591313040065](https://doi.org/10.3103/s0884591313040065)
- Zhou, S., Gügercioğlu, E., Yuan, J., Ge, M., & Yu, C. 2022, Pulsar Glitches: A Review, arXiv, doi: [10.48550/ARXIV.2211.13885](https://arxiv.org/abs/2211.13885)

# Appendix A

## Code

```
def fft_rescale(fourier_trans, window=21):

    from scipy.ndimage import gaussian_filter1d

    pds = (fourier_trans * fourier_trans.conj()).real
    smooth = robust_interp(pds, window // 2 * 2 + 1)
    clip = smooth * 20
    pds[pds > clip] = clip[pds > clip]
    smooth = gaussian_filter1d(pds, 31)
    rescale = 2 / smooth
    return fourier_trans * rescale**0.5

def robust_interp(array, window):

    from scipy.interpolate import interp1d
    from scipy.signal import medfilt

    array = np.array(array)
    array = medfilt(array, window)
    array = np.interp(
        np.arange(len(array)),
        np.arange(len(array))[^np.isnan(array)],
        array[^np.isnan(array)],
    )
    return array
```



# Appendix B

## Pulse profiles

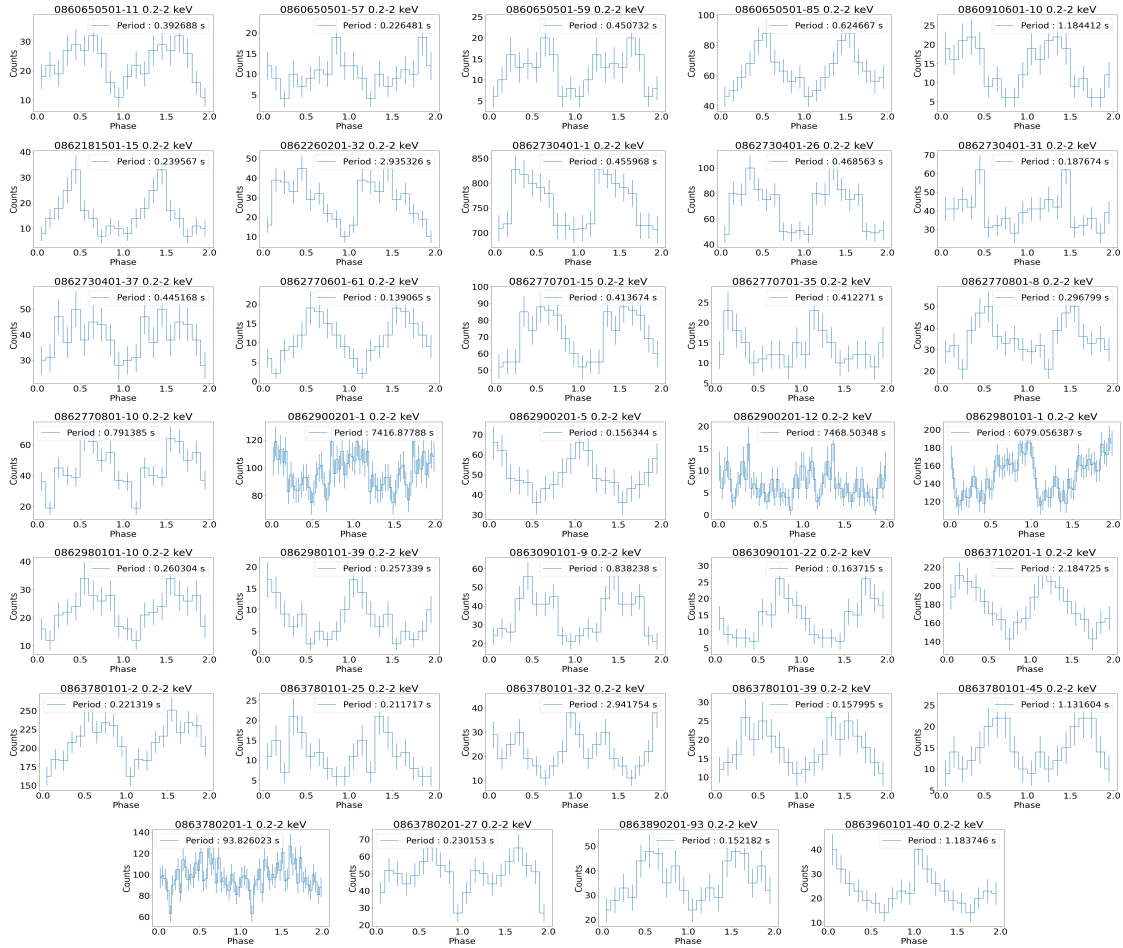


Figure B.1: Pulse profile of the candidates from table 3.1 in the soft X-rays band. They are sorted in the same order as the table, from left to right and from top to bottom.

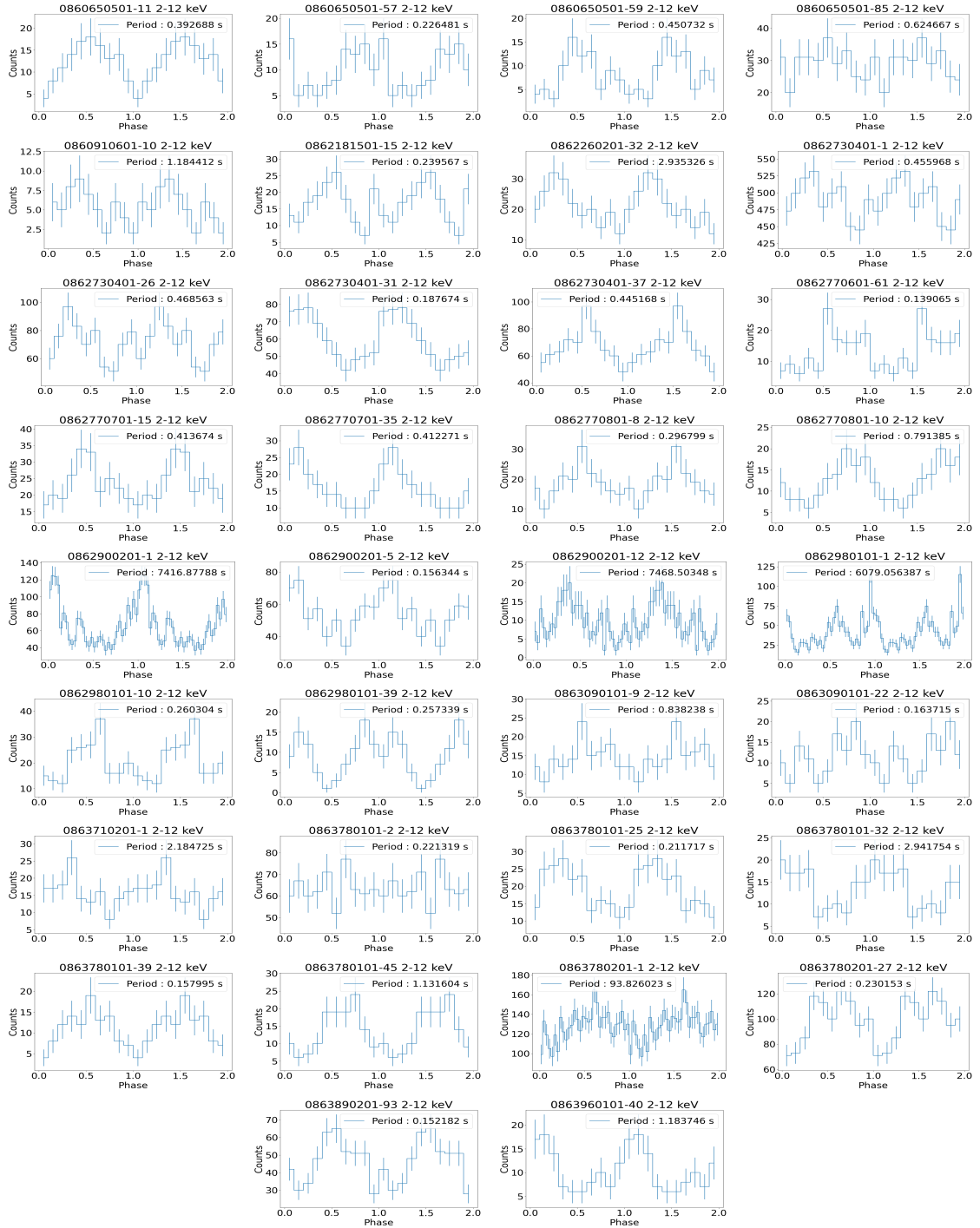


Figure B.2: Pulse profile of the candidates from table 3.1 in the hard X-rays band. They are sorted in the same order as the table, from left to right and from top to bottom.

# Appendix C

## Pulsar emission geometry

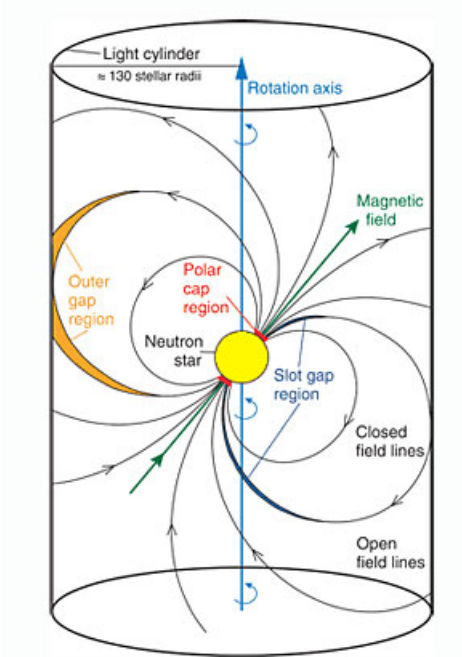


Figure C.1: Pulsar emission geometry. Credits : MAGIC Collaboration